Baroclinic Instability in Vertically Discrete Systems*

AKIO ARAKAWA AND SHRINIVAS MOORTHI**

Department of Atmospheric Sciences, University of California, Los Angeles, California

(Manuscript received 19 August 1987, in final form 21 December 1987)

ABSTRACT

Two vertically discrete systems, one based on the "Charney–Phillips grid" and the other on the "Lorenz grid," are compared in view of the quasi-geostrophic potential vorticity equation and baroclinic instability.

It is shown that with the Charney–Phillips grid, the standard grid for the quasi-geostrophic system of equations, one can easily maintain important dynamical constraints on quasi-geostrophic flow, such as the conservation of quasi-geostrophic potential vorticity through horizontal advection and resulting integral constraints. With the Lorenz grid, however, in which horizontal velocity and (potential) temperature are carried at same levels, it is not straightforward even to define quasi-geostrophic potential vorticity. Moreover, due to an extra degree of freedom in potential temperature, the Lorenz grid can falsely satisfy the necessary condition for baroclinic instability near the lower and upper boundaries. In fact, eigenvalue solutions of the linearized quasi-geostrophic equations show the existence of spuriously amplifying modes with short wavelengths, one trapped near the lower boundary and the other near the upper boundary. The former grows more rapidly than the latter when static stability increases with height. In a model discretized both in vertical and horizontal, the spurious amplification appears with *high* horizontal resolution unless vertical resolution is very high.

The existence of the spurious amplification of short waves in a nonlinear primitive equation model is also confirmed. Here the amplification also influences longer waves through nonlinearity and upper levels presumably through vertical propagation of gravity waves.

It is shown that the spurious amplification can be removed at its origin by introducing additional terms in the thermodynamic equations for the bottom and top layers, which effectively eliminate the possibility of falsely satisfying the necessary condition for baroclinic instability.

1. Introduction

In numerical modeling of a continuous system such as the atmosphere, one must discretize governing differential equations to obtain a finite set of algebraic equations. Discretizations are often used also in theoretical studies to derive simpler dynamical systems. In either case, one hopes that the essential dynamical features of the continuous system are not modified by discretization.

In discretizing differential equations, one is usually guided by basic concepts in numerical analysis such as consistency, order of accuracy and computational stability. In many cases, however, these concepts alone do not provide sufficient guidance in constructing a discrete system whose dynamics closely mimics that of the continuous system. For these cases physical considerations of the dynamics of discrete systems, such as conservation of enstrophy (and kinetic energy) for two-dimensional incompressible flow (Arakawa 1966; Arakawa and Lamb 1977, §IIIB) and of potential enstrophy (and total energy) for shallow-water flow (Arakawa and Lamb 1981) can provide additional guidance.

For modeling the three-dimensional atmosphere, the problem of vertical discretization can be even more important than that of horizontal discretization. In one of his pioneering papers, Lorenz (1960) derived a vertically discrete version of the balanced system of equations that maintains conservation of total energy, mean potential temperature and potential temperature variance under adiabatic processes. In doing so, Lorenz departed from the standard grid for quasi-geostrophic models, referred to as the "Charney–Phillips grid", by introducing a new grid, referred to as the "Lorenz grid" in this paper. In contrast to the Charney–Phillips grid, the Lorenz grid carries horizontal velocity and potential temperature at same levels.

The Lorenz grid is being widely used in existing general circulation and numerical weather prediction models. In particular, Lorenz's approach of conserving total energy, mean potential temperature and potential temperature variance was followed by Arakawa (1972) (see also Arakawa and Lamb 1977) in designing a ver-

* A part of this material was presented in a lecture by the senior author at an ECMWF seminar (Arakawa 1984).

** Present affiliation: Goddard Laboratory for Atmospheres, NASA/Goddard Space Flight Center, Greenbelt, MD 20771.

Corresponding author address: Dr. Akio Arakawa, Dept. of Atmospheric Sciences, University of California, 405 Hilgard Avenue, Los Angeles, CA 90024.

© 1988 American Meteorological Society

tical difference scheme for the primitive equations in a sigma-coordinate. It should be noted, however, that conservations of total energy and potential temperature variance in a discrete model do not necessarily guarantee correct simulations of the conversions from potential energy to kinetic energy and from horizontal potential temperature variance to vertical potential temperature variance. As long as the potential vorticity advection determines the time evolution of flow, we should examine the dynamics of a discrete system from the point of view of potential vorticity.

The purpose of this paper is to advise that care must be taken in constructing a numerical or theoretical model based on the Lorenz grid and in interpreting the results of such a model. Since extratropical large-scale disturbances are nearly quasi-geostrophic regardless of whether the quasi-geostrophic approximation is explicitly used or not in a model, we first concentrate on the quasi-geostrophic system of equations although the Lorenz grid is rarely used for this system. We then confirm the results through numerical integrations of a nonlinear primitive equation model.

Sections 2 and 3 review the quasi-geostrophic system of equations and important integral constraints on quasi-geostrophic motions. Section 4 considers a discrete model based on the Charney–Phillips grid and shows that its dynamics is analogous to that of the continuous system. Problems in discrete models based on the Lorenz grid are discussed in section 5. In particular, we point out that it is not straightforward even to define a discrete version of the quasi-geostrophic potential vorticity with this grid. Section 6 discusses baroclinic instability in two vertically discrete linearized quasi-geostrophic models, one based on the Charney–Phillips grid, the other on the Lorenz grid, showing that short waves can spuriously amplify with the latter grid. Section 7 proposes a simple way to eliminate the spurious amplification at its origin. The existence of the spurious amplification in a nonlinear primitive equation model is confirmed in section 8. Finally, section 9 presents summary and discussion.

2. The quasi-geostrophic system of equations

When the pressure p is used as the vertical coordinate, the quasi-geostrophic system of equations under frictionless and adiabatic processes consists of the following equations:

$$(\partial/\partial t + \mathbf{v}_g\cdot\nabla)(\nabla^2\psi + f) - f_0\frac{\partial\omega}{\partial p} = 0, \quad (2.1)$$

$$(\partial/\partial t + \mathbf{v}_g\cdot\nabla)\frac{\partial\psi}{\partial p} + \frac{\omega}{f_0}S = 0. \quad (2.2)$$

Here $\partial/\partial t$ and ∇ are the time derivative and horizontal gradient operators, respectively, under constant pressure; $\mathbf{v}_g$ is the geostrophic velocity, $\mathbf{k}\times\nabla\psi$; $\mathbf{k}$ is the vertical unit vector; ψ is the geostrophic streamfunction, ϕ/f_0; ϕ is the geopotential gz; g is the gravitational acceleration; z is height; f_0 is a characteristic value of the Coriolis parameter f; ω is the material time derivative of the pressure; S is a static stability parameter defined by $S \equiv -(\alpha/\theta)d\bar{\theta}/dp$; α is the specific volume; θ the potential temperature; and $\bar{\theta}$ a standard potential temperature depending on p only.

Eliminating ω between (2.1) and (2.2), we obtain

$$(\partial/\partial t + \mathbf{v}_g\cdot\nabla)q = 0, \quad (2.3)$$

where q is the quasi-geostrophic "potential vorticity" defined by

$$q \equiv \nabla^2\psi + f + f_0{}^2\frac{\partial}{\partial p}\left(\frac{1}{S}\frac{\partial\psi}{\partial p}\right). \quad (2.4)$$

We assume $\omega = 0$ at the upper ($p = p_T$) and lower ($p = p_S$) boundaries, where p_T and p_S are constant. Then from (2.2),

$$(\partial/\partial t + \mathbf{v}_g\cdot\nabla)\frac{\partial\psi}{\partial p} = 0 \quad \text{at} \quad p = p_T, p_S. \quad (2.5)$$

Following Bretherton (1966), we may combine (2.3) and (2.5) into

$$(\partial/\partial t + \mathbf{v}_g\cdot\nabla)\tilde{q} = 0. \quad (2.6)$$

Here $\tilde{q}$ is the generalized quasi-geostrophic potential vorticity, defined by

$$\tilde{q} \equiv q - \left(\frac{f_0{}^2}{S}\frac{\partial\psi}{\partial p}\right)_{p=p_S}\delta(p_S - p) + \left(\frac{f_0{}^2}{S}\frac{\partial\psi}{\partial p}\right)_{p=p_T}\delta(p - p_T), \quad (2.7)$$

where δ is the Dirac delta function. Similar generalization of Ertel's potential vorticity has been made by James and Hoskins (1985). In what follows, $\tilde{q}$ defined by (2.7) is referred to simply as potential vorticity.

Equations corresponding to (2.4) and (2.5) but with height z as the vertical coordinate are

$$q \equiv \nabla^2\psi + f + \frac{f_0{}^2}{\bar{\rho}}\frac{\partial}{\partial z}\left(\frac{\bar{\rho}}{N^2}\frac{\partial\psi}{\partial z}\right), \quad (2.8)$$

where $\bar{\rho}$ is a standard density depending on z only and N is the Brunt–Väisälä frequency given by $N^2 \equiv gd\ln\bar{\theta}/dz = (\bar{\rho}g)^2S$, and

$$(\partial/\partial t + \mathbf{v}_g\cdot\nabla)\frac{\partial\psi}{\partial z} = 0 \quad \text{at} \quad z = z_S, z_T, \quad (2.9)$$

where z_S and z_T are the heights of the lower and upper boundaries, respectively. We note that (2.8) with constant $\bar{\rho}$ and N^2 is *formally* equivalent to (2.4) with constant S.

3. Integral constraints on quasi-geostrophic flow

Before proceeding to the problem of vertical differencing, we briefly review important integral constraints

on quasi-geostrophic flow that should be maintained in a discrete system. For simplicity, we use the β-plane approximation.

Let the Cartesian coordinates on a β-plane be x (directed eastward) and y (directed northward). Using the Jacobian operator, defined by

$$J(a, b) \equiv \frac{\partial a}{\partial x}\frac{\partial b}{\partial y} - \frac{\partial a}{\partial y}\frac{\partial b}{\partial x}, \tag{3.1}$$

we may rewrite (2.3) and (2.5) as

$$\frac{\partial}{\partial t} L(\psi) = J(L(\psi) + f, \psi), \tag{3.2}$$

$$\frac{\partial}{\partial t}\frac{\partial \psi}{\partial p} = J\left(\frac{\partial \psi}{\partial p}, \psi\right) \quad \text{at} \quad p = p_T, p_S. \tag{3.3}$$

Here L is a differential operator, defined by

$$L(\psi) \equiv \nabla^2\psi + f_0^2 \frac{\partial}{\partial p}\left(\frac{1}{S}\frac{\partial \psi}{\partial p}\right). \tag{3.4}$$

From (3.2) and the integral properties of the Jacobian, we obtain

$$\frac{\partial}{\partial t}\frac{1}{2}\overline{[L(\psi) + f]^2} = 0, \tag{3.5}$$

$$\overline{\psi \frac{\partial}{\partial t} L(\psi)} = 0 \tag{3.6}$$

for all p. Here the overbar denotes the horizontal area mean, along an isobaric surface, over a domain that is periodic in x and bounded by rigid vertical walls at two latitudes, along which ψ is independent of x. Equation (3.5) represents conservation of quasi-geostrophic (absolute) potential enstrophy. Similarly, from (3.3),

$$\frac{\partial}{\partial t}\frac{1}{2}\overline{\left(\frac{\partial \psi}{\partial p}\right)^2} = 0, \tag{3.7}$$

$$\overline{\psi \frac{\partial}{\partial t}\frac{\partial \psi}{\partial p}} = 0 \tag{3.8}$$

at $p = p_S, p_T$.

For the domain being considered, (3.5) is equivalent to

$$\frac{\partial}{\partial t}\frac{1}{2}\overline{[L(\psi)]^2} = -\beta f_0^2 \overline{\frac{\partial \psi}{\partial x}\frac{\partial}{\partial p}\left(\frac{1}{S}\frac{\partial \psi}{\partial p}\right)}. \tag{3.9}$$

Integrating (3.9) by parts with respect to p from p_T to p_S, we obtain

$$\frac{\partial}{\partial t}\int_{p_T}^{p_S}\frac{1}{2}\overline{[L(\psi)]^2}\,dp = -\beta f_0^2\left[\frac{1}{S}\overline{\frac{\partial \psi}{\partial x}\frac{\partial \psi}{\partial p}}\right]_{p_T}^{p_S}. \tag{3.10}$$

If $\partial\psi/\partial p$ is constant at $p = p_S$ and $p = p_T$ (i.e., the lower and upper boundaries are isothermal surfaces), (3.10) becomes

$$\frac{\partial}{\partial t}\int_{p_T}^{p_S}\frac{1}{2}\overline{[L(\psi)]^2}\,dp = 0. \tag{3.11}$$

More generally, if we modify the operator $L(\psi)$ to $\tilde{L}(\psi)$ following the modification of q to $\tilde{q}$, we can show that (3.10) can be written as

$$\frac{\partial}{\partial t}\int_{p_T}^{p_S}\frac{1}{2}\overline{[\tilde{L}(\psi)]^2}\,dp = 0. \tag{3.12}$$

Similarly, integrating (3.6) by parts and using (3.8), we find

$$\frac{\partial}{\partial t}\int_{p_T}^{p_S}\overline{\left[\frac{1}{2}(\nabla\psi)^2 + \frac{1}{2}\frac{f_0^2}{S}\left(\frac{\partial \psi}{\partial p}\right)^2\right]}\,dp = 0. \tag{3.13}$$

The first term in the brackets is the kinetic energy of the geostrophic wind per unit mass, while the second term is the available potential energy of the quasi-geostrophic system per unit mass. Charney (1971) developed a theory of geostrophic turbulence based on the analogy of the conservation laws (3.11) and (3.13) to enstrophy and energy conservation for two-dimensional incompressible flow.

4. The Charney–Phillips vertical differencing

Charney and Phillips (1953) introduced a vertically discrete version of the quasi-geostrophic system of equations based on the vertical grid shown by Fig. 1. Here the index l identifies pressure levels. The geostrophic streamfunction ψ is carried at the integer levels, while ω and θ (or $\partial\psi/\partial p$) are carried at the half-integer levels. Correspondingly, (2.1) is applied to the integer levels and (2.2) applied to the half-integer levels. In this paper, this vertical grid is referred to as the Charney–Phillips grid.

By using the simplest centered differencing for $\partial\omega/\partial p$ and $\partial\psi/\partial p$, we may write a discrete version of (2.1) and (2.2) as

$$\frac{\partial}{\partial t}\nabla^2\psi_l = -\mathbf{v}_l\cdot\nabla(\nabla^2\psi_l + f) + f_0\frac{\omega_{l+\frac{1}{2}} - \omega_{l-\frac{1}{2}}}{(\Delta p)_l}$$

$$\text{for} \quad l = 1, 2, \cdots, L, \tag{4.1}$$

$$\frac{\partial}{\partial t}\frac{\psi_{l+1} - \psi_l}{(\Delta p)_{l+\frac{1}{2}}} = -\mathbf{v}_{l+\frac{1}{2}}\cdot\nabla\frac{\psi_{l+1} - \psi_l}{(\Delta p)_{l+\frac{1}{2}}} - \frac{S_{l+\frac{1}{2}}}{f_0}\omega_{l+\frac{1}{2}}$$

$$\text{for} \quad l = 1, 2, \cdots, L-1, \tag{4.2}$$

where the subscript g for $\mathbf{v}$ has been omitted and

$$(\Delta p)_l \equiv p_{l+\frac{1}{2}} - p_{l-\frac{1}{2}}, \quad (\Delta p)_{l+\frac{1}{2}} \equiv p_{l+1} - p_l, \tag{4.3}$$

$$\mathbf{v}_{l+\frac{1}{2}} \equiv \frac{1}{2}(\mathbf{v}_l + \mathbf{v}_{l+1}). \tag{4.4}$$

Since the boundary conditions $\omega_{\frac{1}{2}} = 0$ and $\omega_{L+\frac{1}{2}} = 0$

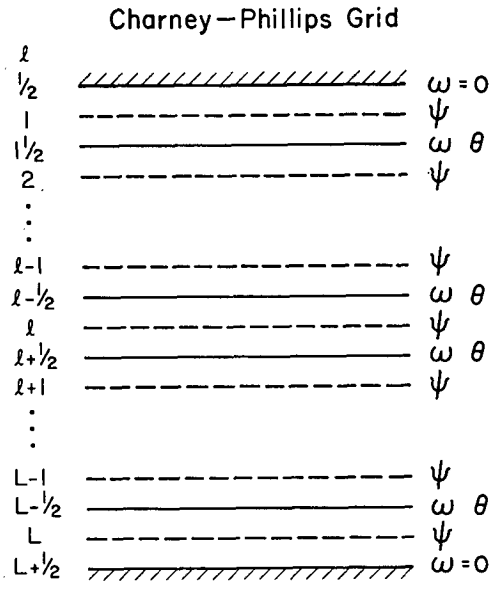

FIG. 1. Vertical grid used by Charney and Phillips (1953).

can be directly incorporated into (4.1) for $l = 1$ and $l = L$, (4.2) applied to $l = 0$ and $l = L$, which corresponds to (2.5), is unnecessary.

Eliminating ω_l for $l = 1\frac{1}{2}, 2\frac{1}{2}, \cdots, L - \frac{1}{2}$ between (4.1) and (4.2), and using $\mathbf{v}_{l+\frac{1}{2}} \cdot \nabla(\psi_{l+1} - \psi_l) = \mathbf{v}_l \cdot \nabla(\psi_{l+1} - \psi_l) = \mathbf{v}_{l+1} \cdot \nabla(\psi_{l+1} - \psi_l)$, we obtain

$$\frac{\partial}{\partial t} \tilde{q}_l = -\mathbf{v}_l \cdot \nabla \tilde{q}_l, \tag{4.5}$$

where

$$\tilde{q}_1 = \nabla^2 \psi_1 + f + \frac{f_0^2}{(\Delta p)_1} \frac{\psi_2 - \psi_1}{(S\Delta p)_{1+\frac{1}{2}}}, \tag{4.6}$$

$$\tilde{q}_l = \nabla^2 \psi_l + f + \frac{f_0^2}{(\Delta p)_l} \left[\frac{\psi_{l+1} - \psi_l}{(S\Delta p)_{l+\frac{1}{2}}} - \frac{\psi_l - \psi_{l-1}}{(S\Delta p)_{l-\frac{1}{2}}} \right]$$

$$\text{for} \quad l = 2, 3, \cdots, L - 1, \tag{4.7}$$

$$\tilde{q}_L = \nabla^2 \psi_L + f - \frac{f_0^2}{(\Delta p)_L} \frac{\psi_L - \psi_{L-1}}{(S\Delta p)_{L-\frac{1}{2}}}. \tag{4.8}$$

It should be noted that (4.7) can be derived from (2.4) through vertical differencing, but (4.6) and (4.8) cannot. This is because the boundary conditions $\omega_{1\frac{1}{2}} = \omega_{L+\frac{1}{2}} = 0$ have already been used in deriving (4.5). Equation (4.5), therefore, is a discrete analog of (2.6) rather than (2.3). In fact, the limit of (4.8), for example, as $(\Delta p)_L$ and $(\Delta p)_{L-\frac{1}{2}}$ approach zero gives

$$\tilde{q}_S = \nabla^2 \psi_S + f - \frac{f_0^2}{p_S - p_{S^-}} \left(\frac{1}{S} \frac{\partial \psi}{\partial p} \right)_{p = p_{S^-}}. \tag{4.9}$$

Here p_{S^-} is the pressure slightly above the surface. This does not agree with the surface value of q defined by (2.4), but it does agree with the surface value of $\tilde{q}$ defined by (2.7). [To see the agreement, integrate (2.7) with respect to p from p_{S^-} to p_S after substitution of q given by (2.4).]

One of the major advantages of the above vertical discretization is that the governing equation can be written in the form of (4.5), which is a discrete analog of (2.6), so that the potential vorticity is well defined. Moreover, the integral constraints presented in section 3 are maintained. From (4.5) through (4.8) we can show

$$\frac{\partial}{\partial t} \frac{1}{2} \Bigg[\overline{\left\{ \nabla^2 \psi_1 + \frac{f_0^2}{(\Delta p)_1} \frac{\psi_2 - \psi_1}{(S\Delta p)_{1+\frac{1}{2}}} \right\}^2} (\Delta p)_1 + \sum_{l=2}^{L-1} \overline{\left\{ \nabla^2 \psi_l + \frac{f_0^2}{(\Delta p)_L} \left(\frac{\psi_{l+1} - \psi_l}{(S\Delta p)_{l+\frac{1}{2}}} - \frac{\psi_l - \psi_{l-1}}{(S\Delta p)_{l-\frac{1}{2}}} \right) \right\}^2} \times \Delta p_l + \overline{\left\{ \nabla^2 \psi_L - \frac{f_0^2}{(\Delta p)_L} \frac{\psi_L - \psi_{L-1}}{(S\Delta p)_{L-\frac{1}{2}}} \right\}^2} \Bigg] \times (\Delta p)_L = 0, \tag{4.13}$$

which is a discrete analog of (3.12). We can also show that this vertical discretization satisfies

$$\frac{\partial}{\partial t} \left[\sum_{l=1}^{L} \frac{1}{2} \overline{(\nabla \psi_l)^2} (\Delta p)_l + \sum_{l=1}^{L-1} \frac{f_0^2}{2} \frac{\overline{(\psi_{l+1} - \psi_l)^2}}{(S\Delta p)_{l+\frac{1}{2}}} \right] = 0, \tag{4.14}$$

which is a discrete analog of (3.13). We may anticipate, therefore, that geostrophic turbulence in this discrete system is analogous to that in the continuous system, provided that horizontal discretization of the Jacobian maintains those integral constraints discussed by Arakawa (1966).

5. The Lorenz vertical differencing

Lorenz (1955, 1960) discussed the concepts of total potential energy, available potential energy and gross static stability, and showed that the balanced model, in which the balance equation (Charney 1955) is used as a filtering approximation, satisfies integral constraints on the quantities mentioned above, the only modification being that the kinetic energy $\frac{1}{2}\mathbf{v}^2$ is replaced by $\frac{1}{2}\mathbf{v}_\psi{}^2$. Here $\mathbf{v}_\psi \equiv \mathbf{k} \times \nabla\psi$ and ψ is the streamfunction satisfying the balance equation. Lorenz (1960) further presented a vertically discrete version of the balanced model, following an approach that could best be described by his own statements quoted here:

> Let us now replace the three-dimensional atmosphere by n layers, bounded by the $n + 1$ isobaric surfaces. . . . We must now replace the system of differential equations by a modified system in which finite differences replace derivatives with respect to p. Our problem is to do this in such a way that reversible adiabatic processes still have numerically equal effects upon ki-

netic energy, total potential energy, available potential energy, and gross static stability. *To this end, we define θ and ψ within each layer. At this point we depart from many of the currently used models in which the wind field is defined at n levels and the temperature field at $n-1$ levels (see Charney and Phillips, 1953).*

Figure 2 shows the vertical grid on which the Lorenz vertical differencing is based. In this paper, this vertical grid is referred to as the Lorenz grid. In this grid, ψ, ϕ and θ are defined for each layer, which is identified by an integer value of l, while ω is carried at each level separating the layers, which is identified by a half-integer value of l. The values of ψ and θ at the internal half-integer levels must be specified through some interpolations between the layers. Lorenz chose

$$\psi_{l+\frac{1}{2}} = \frac{1}{2}(\psi_l + \psi_{l+1}) \tag{5.1}$$

$$\theta_{l+\frac{1}{2}} = \frac{1}{2}(\theta_l + \theta_{l+1}). \tag{5.2}$$

In addition, he chose

$$\phi_l - \phi_{l+1} = c_p\theta_{l+\frac{1}{2}}[(p_{l+1}/p_0)^\kappa - (p_l/p_0)^\kappa] \tag{5.3}$$

for $l = 1, 2, \cdots, L-1$ and

$$p_l = \frac{1}{2}(p_{l-\frac{1}{2}} + p_{l+\frac{1}{2}}). \tag{5.4}$$

Here c_p is the specific heat at constant pressure, $\kappa \equiv R/c_p$; R is the gas constant and p_0 a standard pressure used in defining θ. The choices (5.1) and (5.3) were made to conserve total energy, while the choice (5.2) was made to conserve θ^2 integrated over the entire mass. Equation (5.3) is a finite-difference analog of the hydrostatic equation written in the form

$$\frac{\partial\phi}{\partial(p/p_0)^\kappa} = -c_p\theta. \tag{5.5}$$

The advantage of the Lorenz grid in maintaining conservation laws for the primitive system of equations has also been recognized (e.g., Arakawa 1972; Arakawa and Lamb 1977). In fact, most existing numerical weather prediction and general circulation models with the primitive equations are based on the Lorenz grid. This grid, however, has some problems as outlined below.

The first problem with the Lorenz grid is the existence of an extra degree of freedom in θ. Consider an L-layer model, which has L degrees of freedom in $\mathbf{v}$. Then there are $L-1$ degrees of freedom in the vertical shear of $\mathbf{v}$ and in ω, and thus there are $L-1$ internal (or baroclinic) modes. With the Lorenz grid, however, there are L degrees of freedom in θ, one of which is coupled with none of the internal modes. The solution associated with this extra degree of freedom does not have a counterpart in the continuous system and may be called "vertical computational mode" (Tokioka 1978; Arakawa 1987). For this mode the thermal-wind

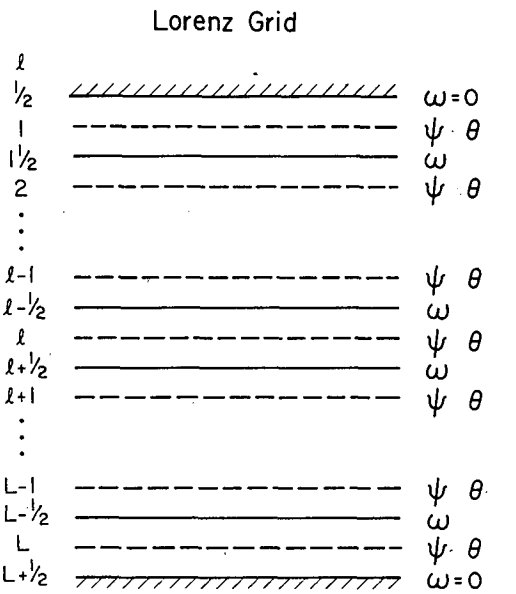

FIG. 2. Vertical grid used by Lorenz (1960).

relationship cannot be satisfied even when it is expected for the continuous case.

The computational mode typically appears as an oscillation of θ from one level to the next, producing a zig-zag vertical profile of θ_l. Possible existence of this oscillation can be illustrated by using (5.2) and (5.3). We see that, because of the averaging in (5.2), $\phi_l - \phi_{l+1}$ given by (5.3) is not affected by superposing $(-1)^l\Delta\theta$ on θ_l, where $\Delta\theta$ is an arbitrary constant. Thus this vertical oscillation of θ is decoupled from the vertical differences of ϕ_l and, therefore, from all internal modes.

It should be noted that the existence of a computational mode is a property of any Lorenz-type grid, in which $\mathbf{v}$ and θ are carried at same levels. One might think that the computational mode can be eliminated by defining ϕ at half-integer levels instead of integer levels and by using the discrete hydrostatic equation such as

$$\phi_{l-\frac{1}{2}} - \phi_{l+\frac{1}{2}} = c_p\theta_l[(p_{l+\frac{1}{2}}/p_0)^\kappa - (p_{l-\frac{1}{2}}/p_0)^\kappa] \tag{5.6}$$

instead of (5.3). Now the discrete hydrostatic equation does not involve averaging of θ_l. For the pressure gradient force at level l, however, we must obtain ϕ_l by averaging $\phi_{l-\frac{1}{2}}$ and $\phi_{l+\frac{1}{2}}$. The difference $\phi_l - \phi_{l+1}$ again depends on an average, though not necessarily arithmetic, of θ_l and θ_{l+1}. Thus the computational mode can still appear (Arakawa 1987).

The second problem with the Lorenz grid is a reduction of the effective static stability, which is most apparent in a two-level model as noted by Hollingsworth (1975). In the continuous case, the continuity equation and the flux form of the thermodynamic equation are given by

$$\nabla \cdot \mathbf{v} + \frac{\partial \omega}{\partial p} = 0 \qquad (5.7)$$

$$\frac{\partial \theta}{\partial t} + \nabla \cdot (\mathbf{v}\theta) + \frac{\partial (\omega\theta)}{\partial p} = 0, \qquad (5.8)$$

respectively. We may write discrete versions of these equations as

$$\nabla \cdot \mathbf{v}_l + \frac{\omega_{l+1/2} - \omega_{l-1/2}}{(\Delta p)_l} = 0 \qquad (5.9)$$

$$\frac{\partial \theta_l}{\partial t} + \nabla \cdot (\mathbf{v}_l \theta_l) + \frac{\omega_{l+1/2}\theta_{l+1/2} - \omega_{l-1/2}\theta_{l-1/2}}{(\Delta p)_l} = 0. \qquad (5.10)$$

Subtracting $\theta_l \times$ (5.9) from (5.10), we obtain

$$(\partial/\partial t + \mathbf{v}_l \cdot \nabla)\theta_l + \frac{1}{(\Delta p)_l}[\omega_{l+1/2}(\theta_{l+1/2} - \theta_l) + \omega_{l-1/2}(\theta_l - \theta_{l-1/2})] = 0, \qquad (5.11)$$

which is a discrete version of the thermodynamic equation written in the advective form. When (5.2) is used to specify θ at half-integer levels, (5.11) becomes

$$(\partial/\partial t + \mathbf{v}_l \cdot \nabla)\theta_l + \frac{1}{(\Delta p)_l}\frac{1}{2}[\omega_{l+1/2}(\theta_{l+1} - \theta_l) + \omega_{l-1/2}(\theta_l - \theta_{l-1})] = 0. \qquad (5.12)$$

For a two-level model as shown in Fig. 3, (5.12) applied to levels 1 and 2 are

$$(\partial/\partial t + \mathbf{v}_1 \cdot \nabla)\theta_1 + \frac{1}{2}\omega_{1\frac{1}{2}}\left(\frac{d\theta}{dp}\right)_{1\frac{1}{2}} = 0 \qquad (5.13)$$

$$(\partial/\partial t + \mathbf{v}_2 \cdot \nabla)\theta_2 + \frac{1}{2}\omega_{1\frac{1}{2}}\left(\frac{d\theta}{dp}\right)_{1\frac{1}{2}} = 0, \qquad (5.14)$$

where

$$\left(\frac{d\theta}{dp}\right)_{1\frac{1}{2}} \equiv \frac{\theta_2 - \theta_1}{\Delta p}. \qquad (5.15)$$

Here $\omega_l = 0$ for $l = \frac{1}{2}, 2\frac{1}{2}$ has been used. We may interpret the factor $\frac{1}{2}$ on $\omega_{1\frac{1}{2}}$ in (5.13) and (5.14) as a consequence of applying the thermodynamic equation to the dashed line levels in Fig. 3, at which ω can be approximated by $\frac{1}{2}\omega_{1\frac{1}{2}}$. If we neglect $(\mathbf{v}_1 - \mathbf{v}_2) \cdot \nabla(\theta_1 - \theta_2)$, the average of (5.13) and (5.14) with (5.2) gives

$$(\partial/\partial t + \mathbf{v}_{1\frac{1}{2}} \cdot \nabla)\theta_{1\frac{1}{2}} + \frac{1}{2}\omega_{1\frac{1}{2}}\left(\frac{d\theta}{dp}\right)_{1\frac{1}{2}} = 0. \qquad (5.16)$$

Note that $\theta_{1\frac{1}{2}}$ is the potential temperature that determines $\phi_1 - \phi_2$ through (5.3). From (5.16) we see that the effective static stability in the two-level model with the Lorenz grid is one-half of that given by (5.15), which is evaluated by a centered difference at level $1\frac{1}{2}$. Similar reduction of the effective static stability appears for the bottom and top layers of a multilayer model.

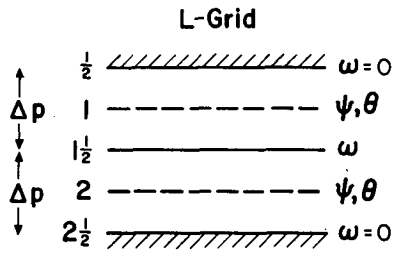

FIG. 3. A two-level model based on the Lorenz grid.

The third problem with the Lorenz grid can be illustrated by applying the grid to the quasi-geostrophic system of equations. Unlike the case of the Charney–Phillips grid, the governing equations with the Lorenz grid cannot be written in the form of (4.5). Consequently, there is no well-defined potential vorticity with this grid. We may define, however, a "potential vorticity *equation*" by a linear combination of the vorticity and thermodynamic equations in which internal ω is eliminated. In an L-layer model with the Lorenz grid, there are L vorticity equations and L thermodynamic equations. If we eliminate $L - 1$ internal ω from these $2L$ equations, we obtain $L + 1$ potential vorticity equations, while there are only L vorticity equations. This increase in the number of potential vorticity equations again comes from the extra degree of freedom in θ.

The potential vorticity equations in the above sense can be obtained by using $\omega_{\frac{1}{2}} = \omega_{L+\frac{1}{2}} = 0$ and eliminating ω_l for $l = 1\frac{1}{2}, 2\frac{1}{2}, \cdots, L - \frac{1}{2}$ between (4.1) and (5.12). The results are

$$\frac{D_1}{Dt}(\zeta_1 + f) - \frac{2f_0}{\Delta p}\frac{1}{\sigma_{1\frac{1}{2}}}\frac{D_1\theta_1}{Dt} = 0, \qquad (5.17)$$

$$\frac{\sigma_{2\frac{1}{2}}}{\sigma_{2\frac{1}{2}} + \sigma_{1\frac{1}{2}}}\frac{D_2}{Dt}(\zeta_2 + f) - \frac{2f_0}{\Delta p}\left[\frac{1}{\sigma_{2\frac{1}{2}} + \sigma_{1\frac{1}{2}}}\frac{D_2\theta_2}{Dt} - \frac{1}{\sigma_{1\frac{1}{2}}}\frac{D_1\theta_1}{Dt}\right] = 0, \qquad (5.18)$$

$$\frac{\sigma_{l+1\frac{1}{2}}}{\sigma_{l+1\frac{1}{2}} + \sigma_{l+\frac{1}{2}}}\frac{D_{l+1}}{Dt}(\zeta_{l+1} + f) + \frac{\sigma_{l-\frac{1}{2}}}{\sigma_{l+\frac{1}{2}} + \sigma_{l-\frac{1}{2}}}\frac{D_l}{Dt} \times (\zeta_l + f) - \frac{2f_0}{\Delta p}\left[\frac{1}{\sigma_{l+1\frac{1}{2}} + \sigma_{l+\frac{1}{2}}}\frac{D_{l+1}\theta_{l+1}}{Dt} - \frac{1}{\sigma_{l+\frac{1}{2}} + \sigma_{l-\frac{1}{2}}}\frac{D_l\theta_l}{Dt}\right] = 0$$

$$\text{for} \quad l = 2, 3, \cdots, L - 2, \qquad (5.19)$$

$$\frac{\sigma_{L-1\frac{1}{2}}}{\sigma_{L-\frac{1}{2}} + \sigma_{L-1\frac{1}{2}}}\frac{D_{L-1}}{Dt}(\zeta_{L-1} + f) - \frac{2f_0}{\Delta p}\left[\frac{1}{\sigma_{L-\frac{1}{2}}}\frac{D_L\theta_L}{Dt} - \frac{1}{\sigma_{L-\frac{1}{2}} + \sigma_{L-1\frac{1}{2}}}\frac{D_{L-1}\theta_{L-1}}{Dt}\right] = 0, \qquad (5.20)$$

$$\frac{D_L}{Dt}(\zeta_L + f) + \frac{2f_0}{\Delta p}\frac{1}{\sigma_{L-\frac{1}{2}}}\frac{D_L\theta_L}{Dt} = 0. \quad (5.21)$$

Here

$$\frac{D_l}{Dt} \equiv \frac{\partial}{\partial t} + \mathbf{v}_l \cdot \nabla, \quad (5.22)$$

$$\sigma_{l+\frac{1}{2}} \equiv -\frac{\bar{\theta}_{l+1} - \bar{\theta}_l}{\Delta p}, \quad (5.23)$$

and $\zeta_l \equiv \nabla^2\psi_l$. For simplicity, Δp has been assumed constant. (To be consistent with the quasi-geostrophic approximation, θ is replaced by $\bar{\theta}$ in (5.23).) Except for (5.17) and (5.21), these potential vorticity equations do not have the form of (4.5); thus there is little hope to maintain the integral constraints discussed in section 3. One cannot even define a discrete version of the potential vorticity unless a crude approximation such as that given below is used.

Let us consider (5.17) through (5.21) for a sufficiently small Δp. Then,

$$\frac{D_{l+1}}{Dt} \doteq \frac{D_l}{Dt} \quad (5.24)$$

may be used *within* each of the potential vorticity equations. We then obtain the following approximate expressions for the potential vorticity with the Lorenz grid:

$$\tilde{q}_1 = \zeta_1 + f - \frac{2f_0}{\Delta p}\frac{\theta_1}{\sigma_{1\frac{1}{2}}}, \quad (5.25)$$

$$\tilde{q}_{1\frac{1}{2}} = \frac{\sigma_{2\frac{1}{2}}}{\sigma_{2\frac{1}{2}} + \sigma_{1\frac{1}{2}}}(\zeta_2 + f) - \frac{2f_0}{\Delta p}\left[\frac{\theta_2}{\sigma_{2\frac{1}{2}} + \sigma_{1\frac{1}{2}}} - \frac{\theta_1}{\sigma_{1\frac{1}{2}}}\right], \quad (5.26)$$

$$\tilde{q}_{l+\frac{1}{2}} = \frac{\sigma_{l+1\frac{1}{2}}}{\sigma_{l+1\frac{1}{2}} + \sigma_{l+\frac{1}{2}}}(\zeta_{l+1} + f) + \frac{\sigma_{l-\frac{1}{2}}}{\sigma_{l+\frac{1}{2}} + \sigma_{l-\frac{1}{2}}}(\zeta_l + f) - \frac{2f_0}{\Delta p}\left[\frac{\theta_{l+1}}{\sigma_{l+1\frac{1}{2}} + \sigma_{l+\frac{1}{2}}} - \frac{\theta_l}{\sigma_{l+\frac{1}{2}} + \sigma_{l-\frac{1}{2}}}\right]$$

$$\text{for} \quad l = 2, 3, \cdots, L-2, \quad (5.27)$$

$$\tilde{q}_{L-\frac{1}{2}} = \frac{\sigma_{L-1\frac{1}{2}}}{\sigma_{L-\frac{1}{2}} + \sigma_{L-1\frac{1}{2}}}(\zeta_{L-1} + f) - \frac{2f_0}{\Delta p}\left[\frac{\theta_L}{\sigma_{L-\frac{1}{2}}} - \frac{\theta_{L-1}}{\sigma_{L-\frac{1}{2}} + \sigma_{L-1\frac{1}{2}}}\right], \quad (5.28)$$

$$\tilde{q}_L = (\zeta_L + f) + \frac{2f_0}{\Delta p}\frac{\theta_L}{\sigma_{L-\frac{1}{2}}}. \quad (5.29)$$

It should be noted that in the limit as $\Delta p \to 0$, (5.29) involves the delta function, as (4.8) for the Charney–Phillips grid does. The same is true for (5.25). A feature unique to the Lorenz grid appears in (5.26) and (5.28). Equation (5.28), for example, also involves the delta function in the limit as $\Delta p \to 0$, but with a coefficient whose sign is opposite to that in (5.29). (Note that $\theta_{L-1}/(\sigma_{L-\frac{1}{2}} + \sigma_{L-1\frac{1}{2}}) \to \theta_L/2\sigma_{L-\frac{1}{2}}$ as $\Delta p \to 0$.) Consequently, there are double potential vorticity sheets of opposing sign at the lower boundary. A similar situation exists between (5.26) and (5.25) at the upper boundary. Another feature unique to the Lorenz grid is in (5.27). Although it is consistent with $q = \zeta + f - f_0\partial(\theta/\sigma)/\partial p$, where $\sigma \equiv -d\bar{\theta}/dp$, (5.27) involves a weighted sum of the vorticity at two adjacent levels. Consequently, the potential vorticity for the interior of the domain can be more properly defined at the half-integer levels than at the integer levels carrying the vorticity.

6. Baroclinic instability with the Charney–Phillips and Lorenz grids

The argument given toward the end of the last section suggests that there can be significant differences between the dynamics of the two discrete models, one based on the Charney–Phillips grid and the other based on the Lorenz grid, especially when the lower (or upper) boundary condition plays an important role. In this section we compare the two discrete models in view of baroclinic instability of horizontally uniform zonal flow with respect to a small-amplitude quasi-geostrophic wave disturbance. An f-plane and a β-plane, both centered at 45°N, and $p_T = 100$ mb and $p_S = 1000$ mb are used.

When $\tilde{q}$ defined by (2.7) is used, one of the necessary conditions for baroclinic instability (Charney and Stern 1962) applied to the y-independent problem is that $\partial\tilde{Q}/\partial y$ must change sign in vertical. Here $\tilde{Q}$ is $\tilde{q}$ for the basic state and

$$\frac{\partial\tilde{Q}}{\partial y} = \beta - f_0^2\frac{d}{dp}\left(\frac{1}{S}\frac{dU}{dp}\right) + \frac{f_0^2}{S}\left(\frac{dU}{dp}\right)_{p=p_S}\delta(p_S - p) - \frac{f_0^2}{S}\left(\frac{dU}{dp}\right)_{p=p_S}\delta(p - p_T), \quad (6.1)$$

where $U(p)$ is the basic zonal flow (eastward positive). For simplicity, we shall only consider the case dU/dp = constant < 0 (i.e., a profile linear in p with westerly shear) throughout this section. If we further assume that S is constant, the second term on the right-hand side of (6.1) vanishes.

a. $\beta = 0$ and constant S

From (2.4) with constant S and (2.8) with constant $\bar{\rho}$ and $\bar{N}^2$, we see that this case is formally equivalent to the Eady model (Eady 1949). In this model, $\partial\tilde{Q}/\partial y = 0$ except at the boundaries. The necessary condition for instability is then satisfied due to the existence of the two boundary terms in (6.1). For this model, Eady found that one normal mode solution grows for wavelengths longer than a cutoff wavelength, which

depends on static stability. Following an initial-value problem approach, Pedlosky (1964) showed that the growing mode found by Eady is the only growing mode in the model, even though normal modes do not form a complete set.

We have calculated growth rates by solving the linearized, vertically discrete, y-independent, quasi-geostrophic equations as an eigenvalue problem. Figure 4 shows the results for $S = 0.02\ \mathrm{m^2\ s^{-2}\ mb^{-2}}$ obtained from the 2-level, 6-level and 18-level models. [For the Lorenz grid, the vertical differencing of Arakawa and Suarez (1983) was used instead of the original Lorenz vertical differencing. We prescribed $\bar{\theta}$ at integer levels instead of S at half-integer levels. The values of $\bar{\theta}$ are taken from a continuous profile that has the value of S given above with $(\bar{\theta})_{1000\ \mathrm{mb}} = 290$ K and the values of U linear in p prescribed at half-integer levels instead of integer levels. Geostrophic balance and the Arakawa–Suarez vertical differencing then determine θ and U at integer levels for the basic state.] As we can see from the figure, the cutoff wavelength of the 2-level model is shorter with the Lorenz grid than with the Charney–Phillips grid. This is anticipated since the effective static stability is reduced when the Lorenz grid is used (see section 5).

The most striking feature in Fig. 4 is the rapid growth of short waves in multilevel models with the Lorenz grid. This is obviously spurious since short waves in the continuous Eady model are neutral. The maximum of this spurious growth rate shifts toward shorter wave-

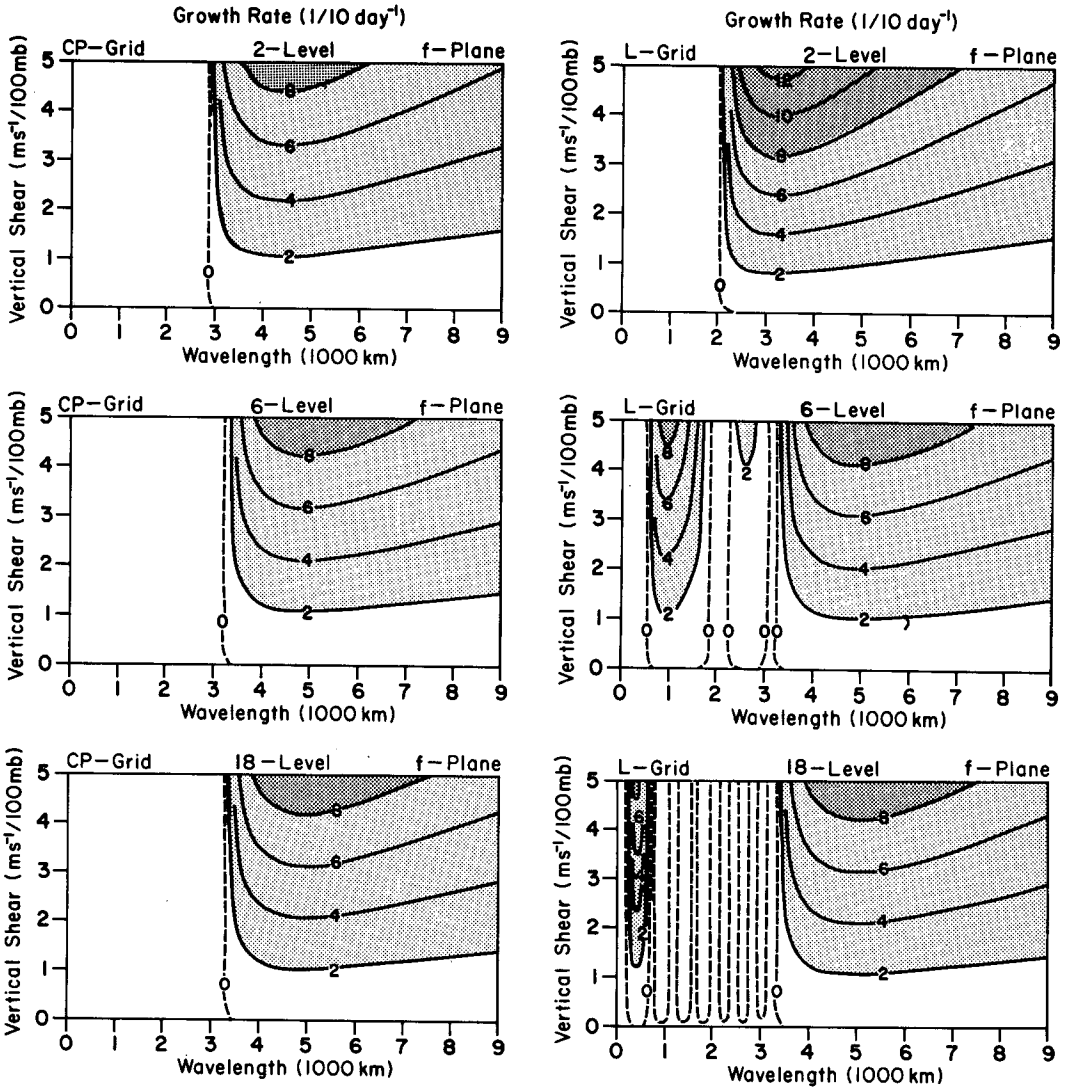

FIG. 4. Growth rates for $\beta = 0$ and constant S as functions of wavelength and vertical shear obtained from the 2-level (upper panels), 6-level (middle panels) and 18-level (lower panels) models based on the Charney–Phillips grid (left panels) and the Lorenz grid (right panels).

lengths as the vertical resolution increases. This can be more clearly seen in Fig. 5, in which the growth rates for $|dU/dp| = 5\ \mathrm{m\ s^{-1}}\ (100\ \mathrm{mb})^{-1}$ are shown as functions of wavelength and the number of levels. Note that the growth rates with the Charney–Phillips grid rapidly converge as the number of levels increases, while those for short waves with the Lorenz grid converge very slowly. Even with the 30-level model, we can see the spurious amplification though it appears for very short wavelengths.

The upper panels of Fig. 6 show the real part of the complex phase speed c, relative to U at the bottom boundary, of various modes in the 18-level models for the same $|dU/dp|$ as functions of wavelength. On the heavy parts of the lines c is a pair of complex conjugates, while on the thin parts c is real. (Since U is linear in p, the ordinate of these panels can be interpreted as the steering-level pressure, with tick marks corresponding to the half-integer levels.) Parallel or nearly parallel thin lines correspond to singular neutral modes in the continuous case. The steering levels of these modes with the Charney–Phillips grid are approximately at $l = 2, 3, \cdots, 17$, while those with the Lorenz grid are approximately at $l = 1\frac{1}{2}, 2\frac{1}{2}, \cdots, 17\frac{1}{2}$. These are the levels where $\tilde{q}$ is defined with $L = 18$ (see (4.7), (5.26), (5.27) and (5.28)). The lower panels of Fig. 6 show the growth rates of amplifying modes. As we can see from the upper panel, amplifying short waves appear as a pair of two modes at a given wavelength, with steering levels approximately symmetric with respect to the middle level. The growth rates of these modes are very close to each other and, therefore, they are not shown separately in the lower panel. Figure 7 shows the structures of selected modes with the Lorenz grid. The upper, middle and lower panels are for the spuriously amplifying mode at the wavelength of 300 km with the lower steering level, the amplifying Eady mode at the wavelength of 5000 km, and the slowest neutral mode at the wavelength of 300 km, respectively.

The existence of the spuriously amplifying modes can be interpreted as a consequence of the failure of the Lorenz grid in simulating $\partial\tilde{Q}/\partial y = 0$ inside the boundaries. In particular, the shortest-wavelength peak, which is the most dominant peak, can be interpreted as a consequence of falsely satisfying the necessary condition for baroclinic instability. This is possible with the Lorenz grid due to the increase in the number of potential vorticity equations. As pointed out in section 5, in the limit as $\Delta p \to 0$, there are double potential vorticity sheets of opposing sign at each boundary. The necessary condition can then be satisfied locally at each boundary. Even when Δp is not infinitesimally small, similar situations can occur between the layers L and $L - 1$ and between the layers 1 and 2. The vertical structure shown in the upper panel of Fig. 7, which is highly trapped near the lower boundary, is consistent with this interpretation.

b. $\beta \neq 0$ and constant S

This case is equivalent to the Green model. As Green (1960) showed, the inclusion of β eliminates the short-wave cutoff of the Eady model. The results for this case are shown in Figs. 8, 9 and 10, which correspond to Figs. 4, 5 and 6 for the f-plane case, respectively. Minor peaks now appear in multilevel models with the Charney–Phillips grid, presumably due to the critical-layer instability with non-zero $\partial Q/\partial y$ (Bretherton 1966). The growth rate spectrum is discrete, however, because there are only discrete critical levels. More importantly,

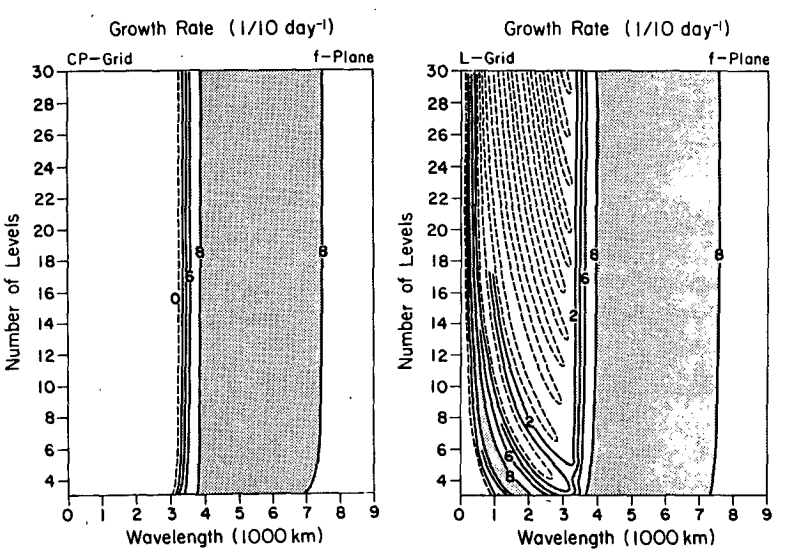

FIG. 5. As in Fig. 4 but as functions of wavelength and number of levels for $|dU/dp| = 5\ \mathrm{m\ s^{-1}}\ (100\ \mathrm{mb})^{-1}$.

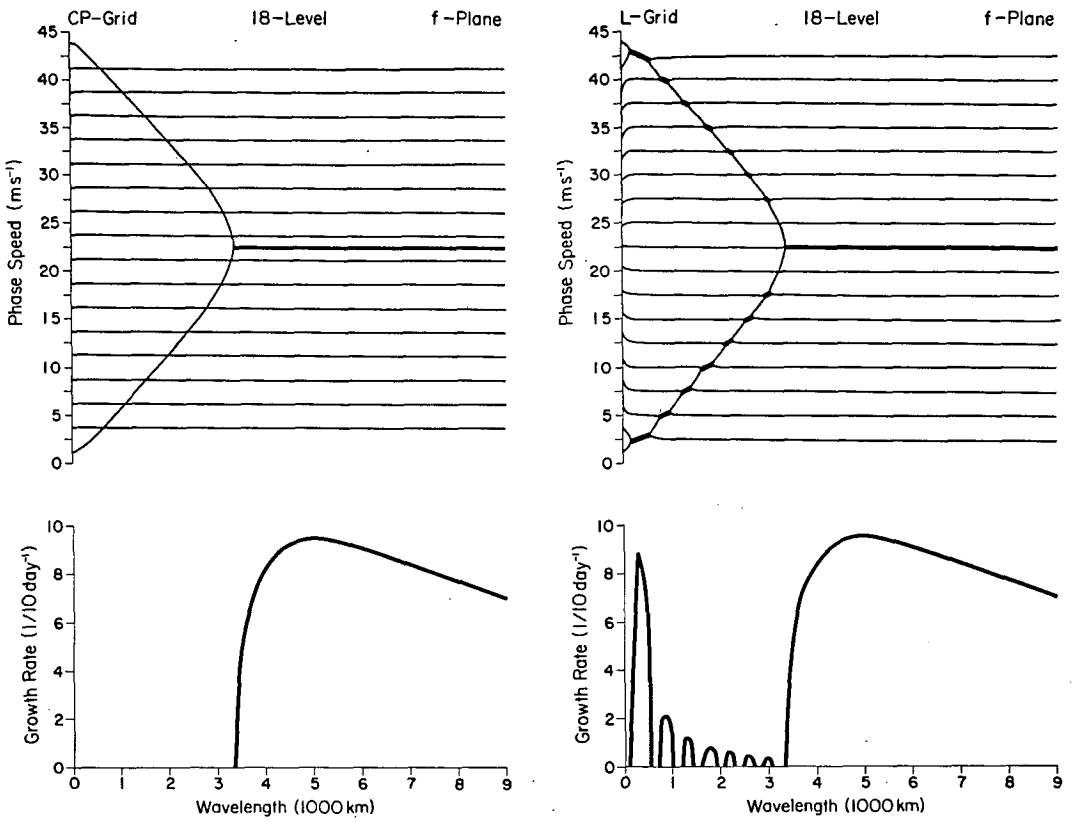

FIG. 6. (The real part of) phase speed (upper panels) and growth rates (lower panels) as functions of wavelength obtained from 18-level models applied to the case shown in Fig. 5.

rapid growth of short waves again appears in multilevel models with the Lorenz grid. The shortest-wavelength peak, which is now slightly different between the upper and lower modes, must be associated with what we found in the f-plane case. (Figures 8 and 9 are based on the largest values of the growth rates at a given wavelength. This applies to all figures showing the growth rates in the rest of this paper.)

c. $\beta \neq 0$ and constant temperature lapse rate

We have performed similar analysis for $\Gamma = 6°C$ km^{-1}, where $\Gamma \equiv -\partial\bar{T}/\partial z$ is the basic temperature lapse rate. As shown in Fig. 11, this state has a more realistic vertical distribution of S, characterized by nearly constant, small values at lower levels and rapidly increasing, large values at upper levels. Owing to this vertical distribution of static stability, the spuriously amplifying mode trapped near the lower boundary should be even more rapidly growing, while that trapped near the upper boundary should be less rapidly growing. The results for this case are shown in Fig. 12, which corresponds to Fig. 9 for the constant S case. Growth rates of the spuriously amplifying mode trapped near the upper boundary are now considerably small (less than $1.5 \times {}^{1}/_{10}$ day^{-1}) and, therefore, they do not appear in Fig. 12. Growth rates with the Lorenz grid are shown also in Fig. 13a, using wavenumber as abscissa for the wavelength range 200 km through 3000 km, to see the growth rates for short waves more clearly. From this figure we find maximum growth rates near 700 km wavelength with the 6-level model, near 400 km wavelength with the 9-level model, and near 200 km wavelength with the 18-level model.

d. The effect of horizontal truncation

Although the use of the Lorenz grid can cause spurious amplification of short waves, they may not be resolved in a horizontally truncated model. Even when resolved, they can be significantly modified by truncation errors due to horizontal finite-differencing. To see this situation quantitatively, we have recalculated the growth rates for the case of section 6c but with all derivatives with respect to x replaced by centered second-order finite differences. Figure 14a–d correspond to Fig. 13a except that the horizontal grid size Δx is now finite. We can see that (i) when $\Delta x = 500$ km, the model cannot resolve any amplification of short waves; (ii) as Δx decreases, the spurious amplification becomes more and more serious unless the number of levels in the vertical is very large; (iii) when $\Delta x = 100$

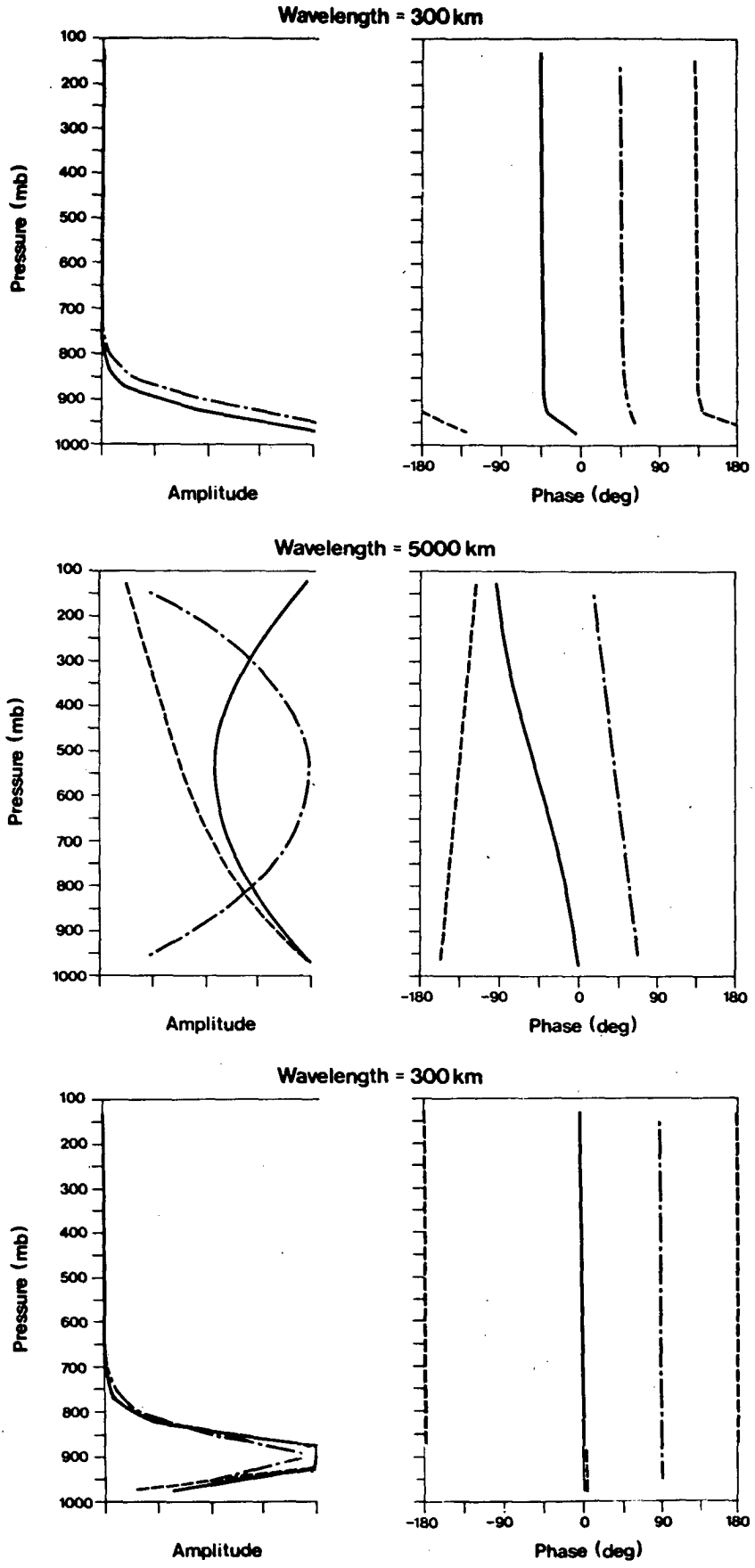

FIG. 7. Amplitudes (left panels) and phase (right panels) of selected modes with the Lorenz grid for the case of Fig. 6. Solid, dashed and chain lines are for ψ, T and ω, respectively. In the top left panel, the dashed and solid lines overlap. See text for further explanations.

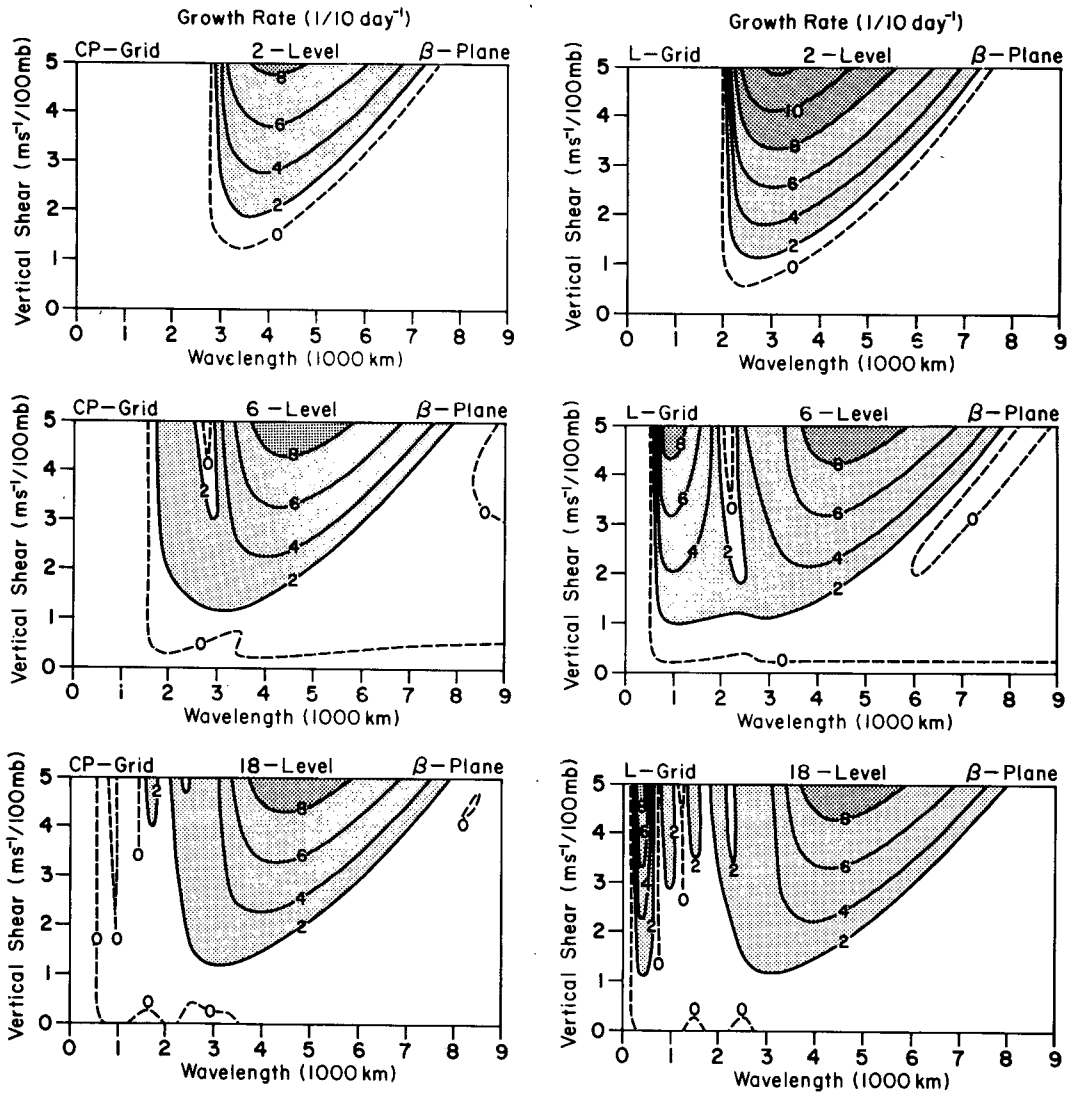

FIG. 8. As in Fig. 4 except for $\beta \neq 0$.

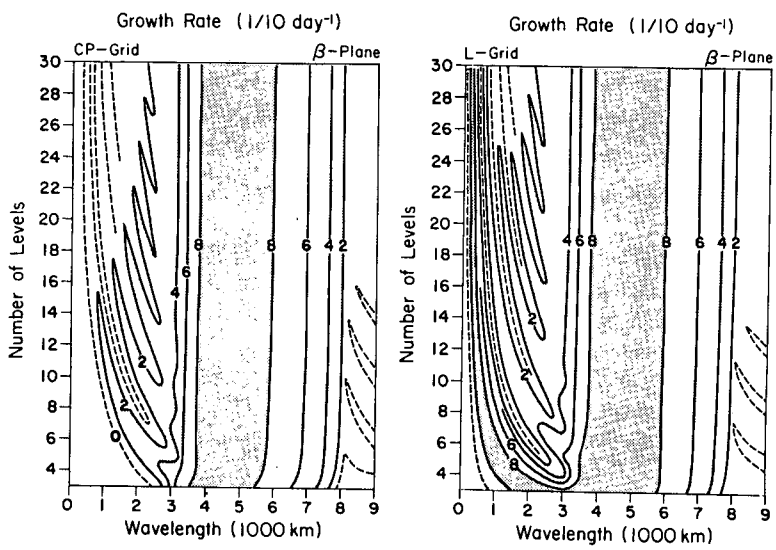

FIG. 9. As in Fig. 5 except for $\beta \neq 0$.

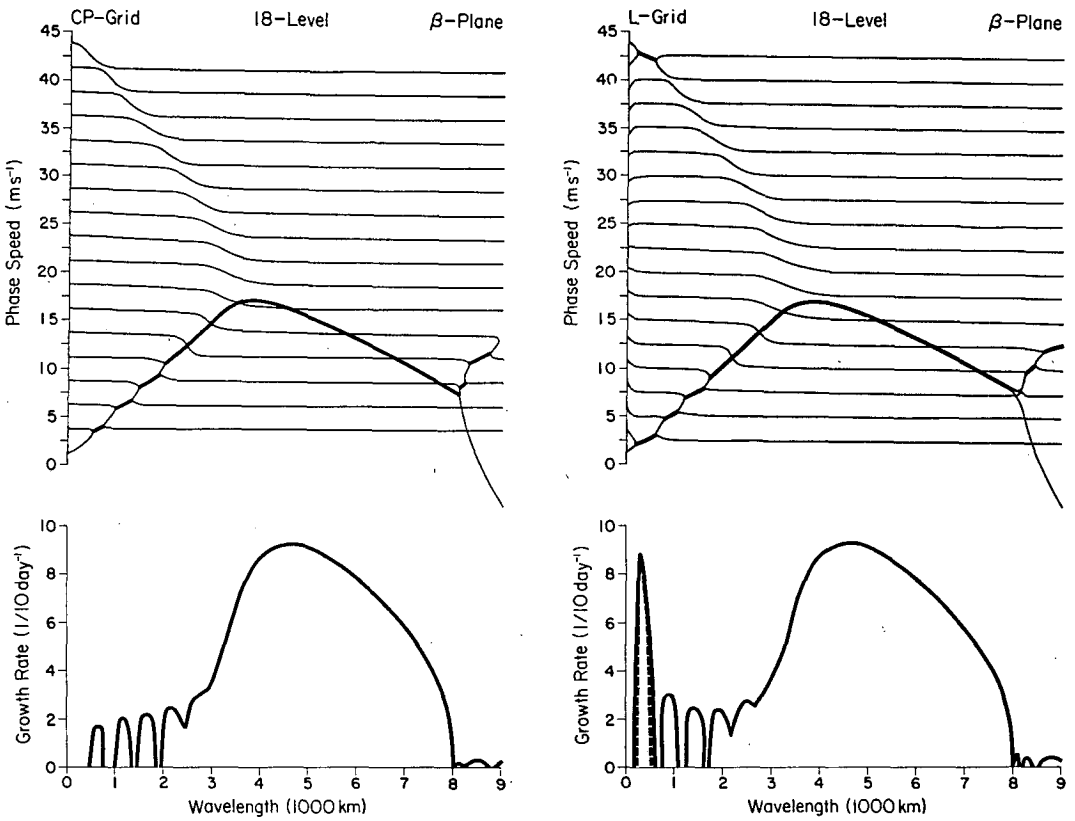

FIG. 10. As Fig. 6 except for $\beta \neq 0$. The dashed line in the lower right panel shows the growth rate of the mode trapped near the upper boundary.

km, even with the 11-level model the growth rates of short waves are comparable to those of long waves and even with the 20-level model they are not negligible. Figure 13a suggests that the situation becomes worse as Δx continues to decrease.

7. Elimination of the spurious amplification of short waves

To obtain further insight into the cause of the spurious amplification of short waves with the Lorenz grid, we have recalculated the growth rates with the additional term

$$-k(\theta_1 - s_1\theta_2) \tag{7.1}$$

on the right-hand side of the $\partial\theta_1/\partial t$ equation and

$$-k(\theta_L - s_L\theta_{L-1}) \tag{7.2}$$

in the right-hand side of the $\partial\theta_L/\partial t$ equation. If we choose $s_1 = \sigma_{1\frac{1}{2}}/(\sigma_{2\frac{1}{2}} + \sigma_{1\frac{1}{2}})$ and $s_L = \sigma_{L-\frac{1}{2}}/(\sigma_{L-\frac{1}{2}} + \sigma_{L-1\frac{1}{2}})$, these terms adjust θ_1 and θ_L in such a way that the quantities inside the brackets in (5.26) and (5.28) remain small as far as the perturbations are concerned. (Note that perturbation equations are the only time-dependent equations in our linearized problem.) More generally, expressions corresponding to (5.26) and (5.28) rederived without (5.2) indicate that s_1 and s_L should be

$$s_1 = \frac{(\bar{\theta}_{1\frac{1}{2}} - \bar{\theta}_1)/(\Delta p)_1}{(\bar{\theta}_{2\frac{1}{2}} - \bar{\theta}_{1\frac{1}{2}})/(\Delta p)_2}, \tag{7.3}$$

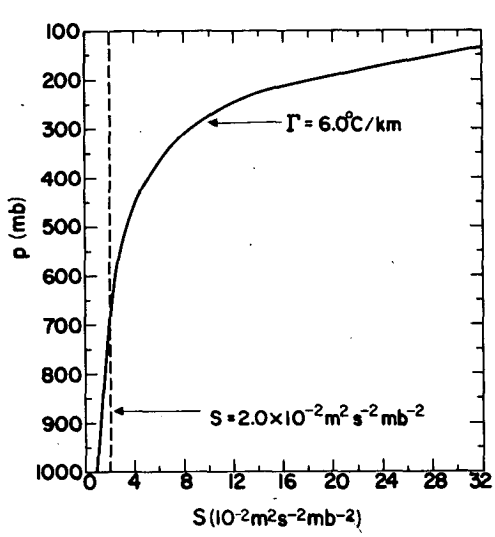

FIG. 11. Vertical profile of the static stability parameter S for temperature lapse rate $\Gamma = 6°C\ km^{-1}$.

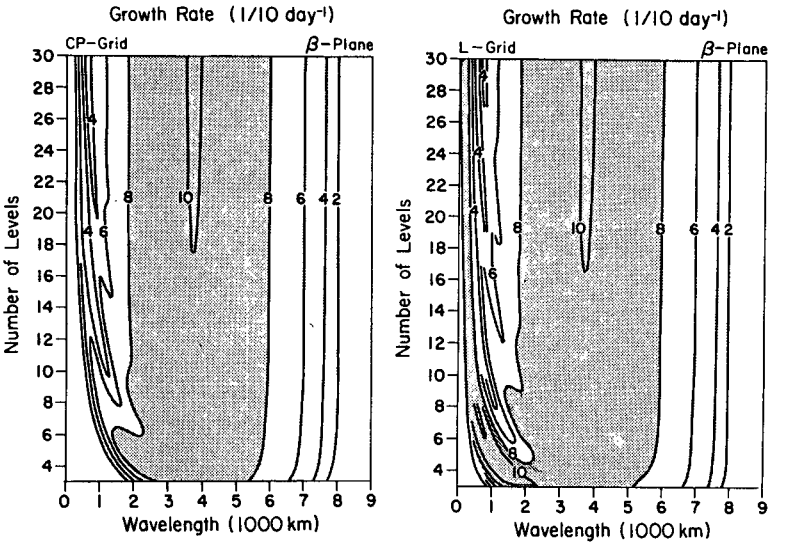

FIG. 12. As in Fig. 5 except for $\beta \neq 0$ and $\Gamma = 6°C\ km^{-1}$.

$$s_L = \frac{(\bar{\theta}_L - \bar{\theta}_{L-\frac{1}{2}})/(\Delta p)_L}{(\bar{\theta}_{L-\frac{1}{2}} - \bar{\theta}_{L-1\frac{1}{2}})/(\Delta p)_{L-1}}. \qquad (7.4)$$

For later convenience, Δp in (7.3) and (7.4) has been allowed to be uneven.

Through growth-rate calculations with (7.1) through (7.4), we found that if $k \geq 10^{-3}\ s^{-1}$, the results are insensitive to changes in k over many orders of magnitude. Figure 13b presents the modified growth rates with $k = 10^{-3}\ s^{-1}$ for the case of section 6c. By comparing Fig. 13b with Fig. 13a, we see that the spuriously amplifying mode is now completely eliminated, while the growth rates for other modes are virtually unaffected. The results are now very similar to those with the Charney–Phillips grid shown in Fig. 12 using wavelength as the abscissa. This suggests that the origin of the spurious amplification with the Lorenz grid is in fact the terms similar to the bracketed terms in (5.26) and (5.28). We have also tried various forms of horizontal and vertical diffusion; but none of them has

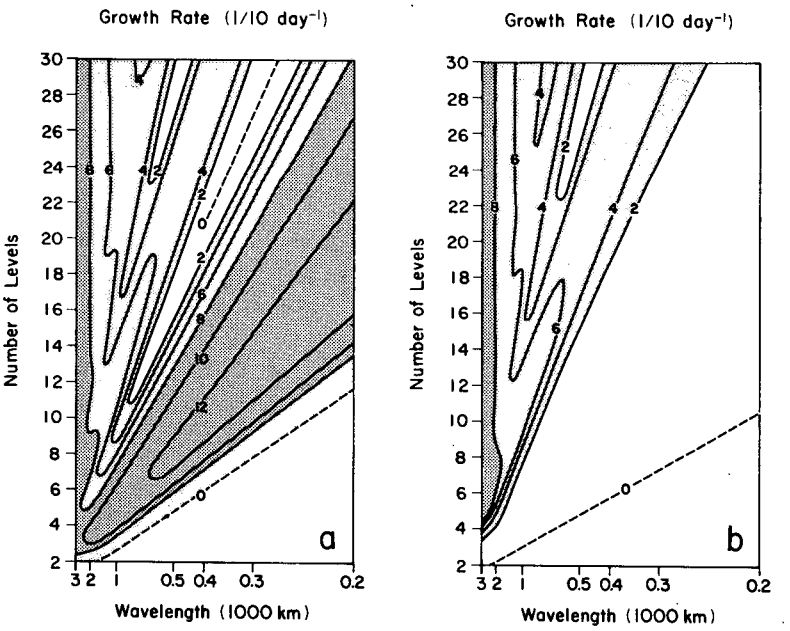

FIG. 13. (a) As in Fig. 12 but using wavenumber as abscissa. (b) As in (a) but with $k = 10^{-3}\ s^{-1}$ in the adjustment terms given by (7.1) and (7.2).

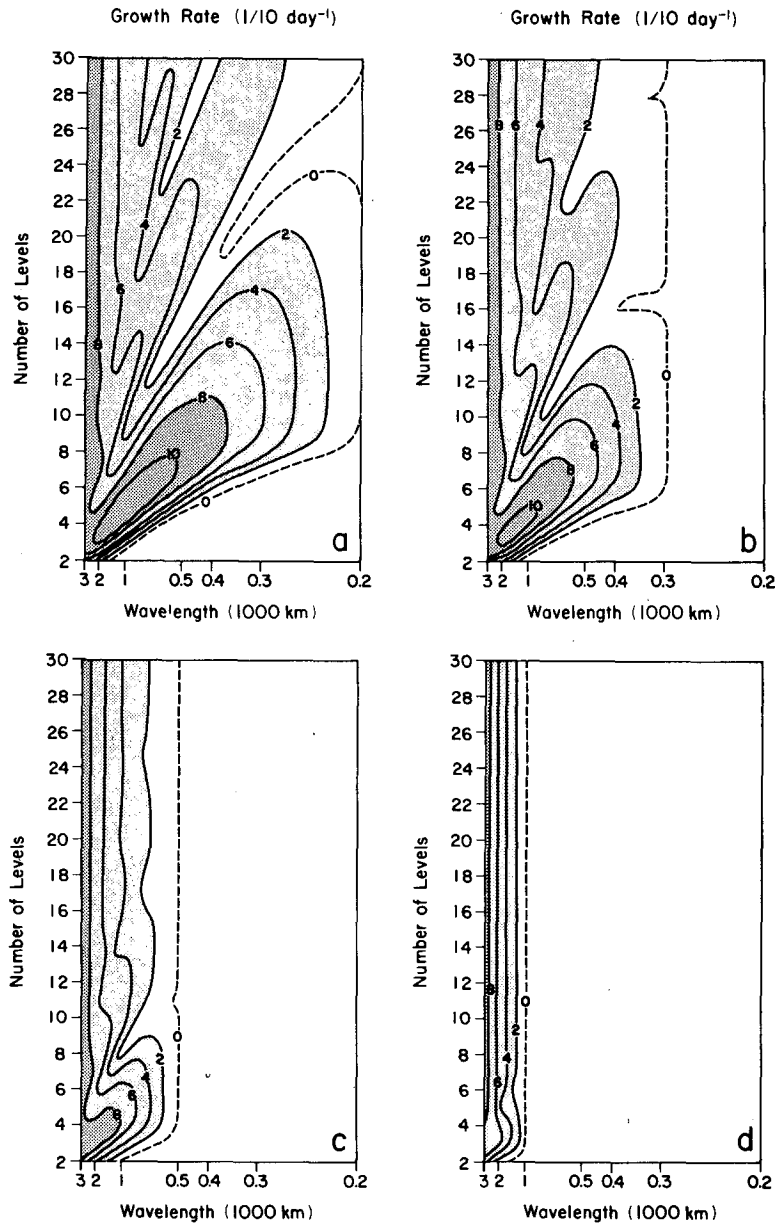

FIG. 14. As in Fig. 13a except for finite horizontal grid sizes (a) 100 km, (b) 150 km, (c) 250 km, and (d) 500 km.

been found to be as effective as the terms (7.1) and (7.2) in eliminating the spurious amplification without affecting the growth of other modes.

To help in interpreting the results of next section, growth rates of y-dependent perturbations with and without the adjustment terms are compared using an eight-layer model on an f-plane with $f = 10^{-4}$ s^{-1} and $\Gamma = 5°$C km^{-1}. The basic flow is still assumed to be uniform both in x and y. Figure 15 shows the vertical structure of the eight-layer model. (See section 5 for the choice of this particular vertical structure.) Figure 16 presents the growth rates for $|dU/dp| = 5$ m s^{-1} (100 mb)$^{-1}$ (a) with $k = 0$ (i.e., without the adjustment terms) and (b) with $k = 10^{-3}$ s^{-1}. We see that the adjustment terms eliminate the growth of waves which have short wavelengths either in x and/or y. Because the static stability for this basic state rapidly increases in height, the adjustment term (7.2) rather than (7.1) is responsible for the difference between Figs. 16a and 16b.

8. Numerical experiments with a nonlinear primitive-equation model

Until now we have demonstrated the existence of spurious amplification of short waves with the Lorenz

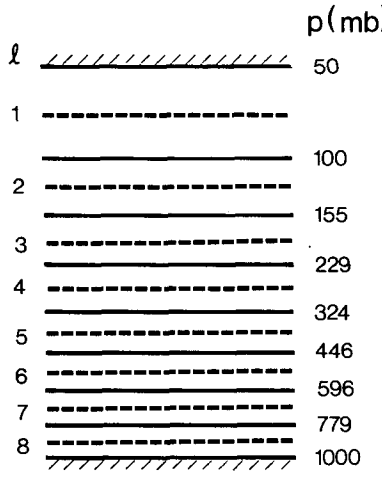

FIG. 15. Vertical structure of the 8-layer model used for the growth-rate calculations shown in Fig. 16.

grid by using the linearized quasi-geostrophic equations. Then two important questions remain to be answered. The first, does such amplification occur when the quasi-geostrophic approximation is not used? The second, what is the role of nonlinearity? To address these two questions, we have performed numerical experiments with a nonlinear primitive-equation model with the Lorenz grid.

The model we have used is an 8-layer model based on a modified version of the σ-coordinate (Phillips 1957) with no surface topography. The vertical structure of the model is the same as that shown in Fig. 15 when the surface pressure $p_s = 1000$ mb. This structure corresponds to that of the 9-layer version of the UCLA GCM (Suarez et al. 1983) when the GCM's variable-depth bottom layer, which represents the planetary boundary layer, is very thin. The vertical differencing follows Arakawa and Suarez (1983) and the horizontal differencing is based on the second-order potential enstrophy conserving scheme (Arakawa and Lamb 1981). No physical process is included except for a Newtonian cooling, which tends to restore the potential temperature toward its initial value with a relaxation time of ten days. The model is applied to a rectangular domain on an f-plane with $f = 10^{-4}$ s^{-1}. In the zonal direction, the domain size is 6000 km with cyclic boundaries and in the meridional direction, the domain size is 9000 km with rigid lateral boundaries. The grid size is 150 km in both directions. Initial condition consists of an area-mean vertical profile of potential temperature corresponding to a constant lapse rate of 5°C km^{-1}, a zonal flow in a geostrophic balance with $p_S = 1000$ mb, and random potential temperature perturbations in the range between ±1°C. The zonal flow has a half-cosine meridional profile, with zeros at the boundaries, and a vertical profile linear in pressure. The maximum vertical shear, which appears at the center of the zonal channel, is 5 m s^{-1} (100 mb)$^{-1}$.

With the initial condition previously described, we performed two 15-day integrations, one without and the other with the adjustment terms given by

$$\nabla \cdot [K(\nabla\theta_1 - s_1\nabla\theta_2)] \tag{8.1}$$

in the right-hand side of $\partial\theta_1/\partial t$ equation and

$$\nabla \cdot [K(\nabla\theta_L - s_L\nabla\theta_{L-1})] \tag{8.2}$$

in the right-hand side of $\partial\theta_L/\partial t$ equation ($L = 8$ for the model used here) with $K = 5 \times 10^6$ m^2 s^{-1}. The coefficients s_1 and s_L are given by (7.3) and (7.4), respectively. Instead of directly using (7.1) and (7.2), the diffusive form was chosen since presently we are not dealing with perturbation equations and we wish to avoid any substantial modification of the "basic" (i.e.,

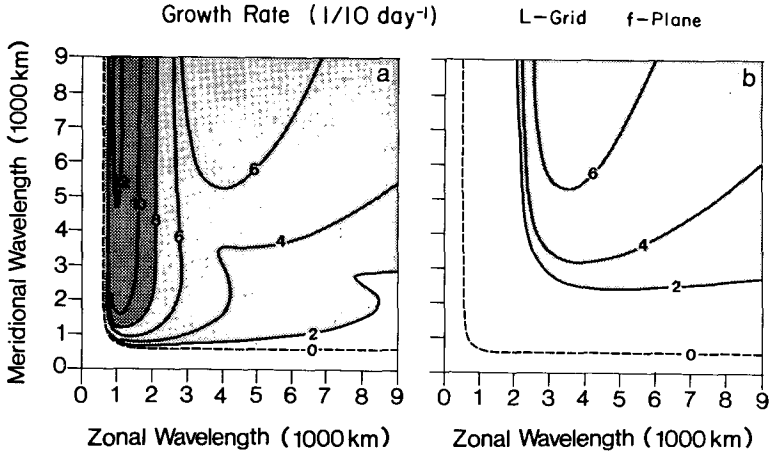

FIG. 16. Growth rates for $\beta = 0$, $|dU/dp| = 5$ m s^{-1} (100 mb)$^{-1}$ and $\Gamma = 5$°C (100 mb)$^{-1}$ as functions of zonal and meridional wavelengths obtained with the 8-layer model shown in Fig. 15: (a) with $k = 0$ and (b) with $k = 10^{-3}$ s^{-1}.

area-averaged) potential temperatures predicted by the model. We have tested (8.1) and (8.2) in some selected linearized quasi-geostrophic cases and found that the results are almost identical to those with (7.1) and (7.2).

Results from the integration without the adjustment terms are shown in Figs. 17, 19 and 21, and those with the adjustment terms are shown in Figs. 18, 20 and 22. Figures 17, 18, 19 and 20 are based on potential temperature variance associated with each horizontal wave component. The variance is first calculated for each of the model layers and then vertically averaged with the weight given by the mean mass of the layers. Figures 17 and 18 show natural logarithm of the variance for $m = 1$ through 5 with (a) $n = 0$ and (b) $n = 5$. Here m and n are zonal and meridional integer wavenumbers for this domain. In Fig. 17 we see more or less linear growth (i.e., exponential growth of the variance) of all waves after an initial adjustment period of a day or two. This is in qualitative agreement with

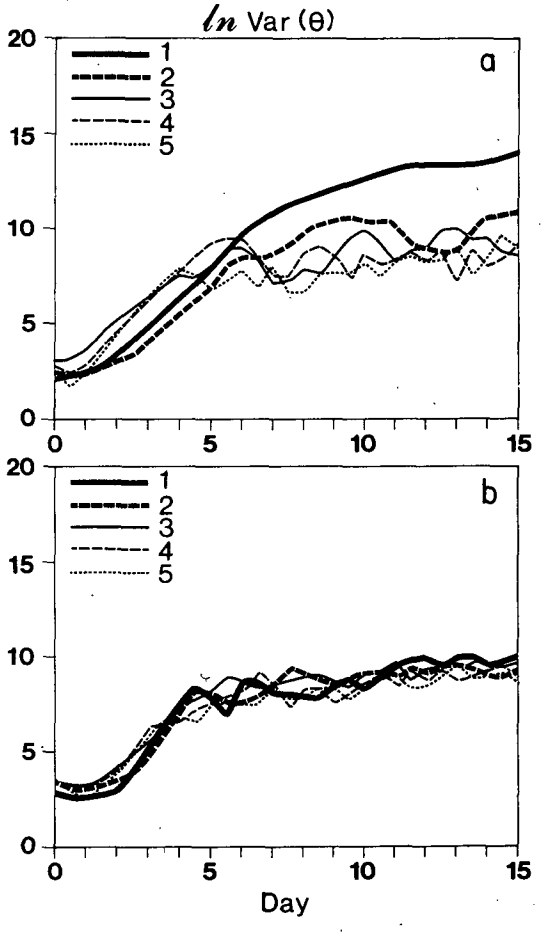

FIG. 17. Natural logarithm of the potential temperature variance as functions of time obtained by the primitive equation model. (a) For zonal wavenumbers 1 through 5 and meridional wavenumber 0. (b) Same as (a) but for meridional wavenumber 5.

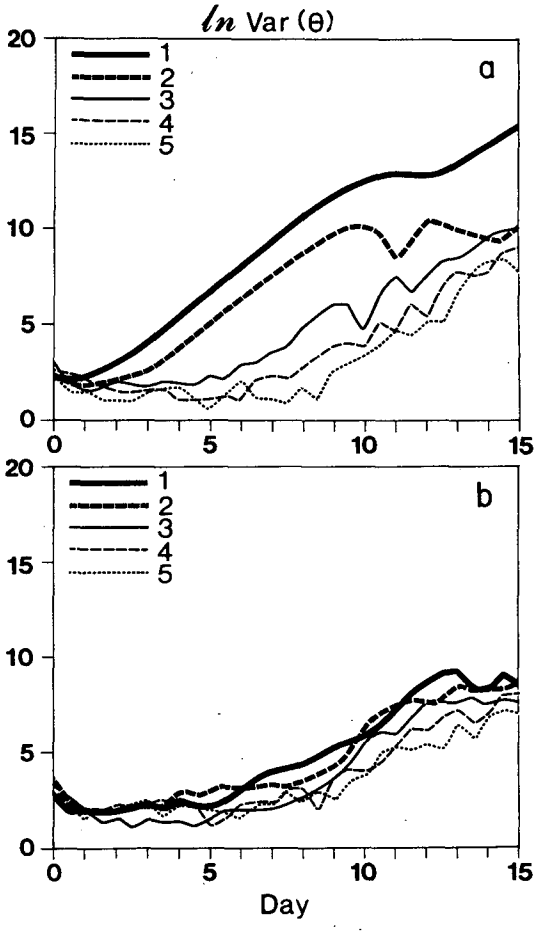

FIG. 18. As in Fig. 17 but with $K = 5 \times 10^6$ m^2 s^{-1} in the adjustment terms (8.1) and (8.2).

the results of linearized quasi-geostrophic model shown in Fig. 16a. After day 4 or 5, most waves enter nonlinear regimes while the longest wave shown by the heavy

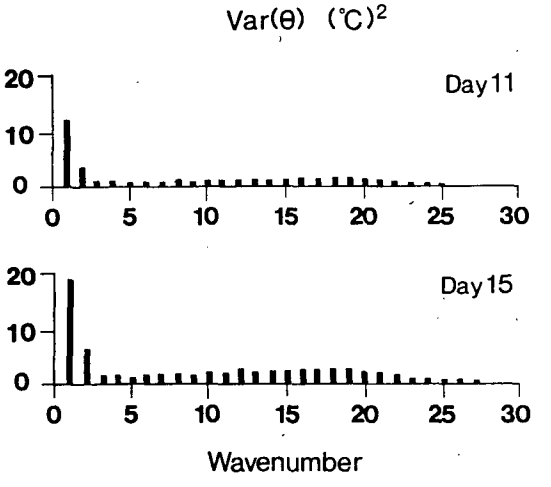

FIG. 19. Spectrum distribution of the potential temperature variance on day 11 and day 15 for the case of Fig. 17.

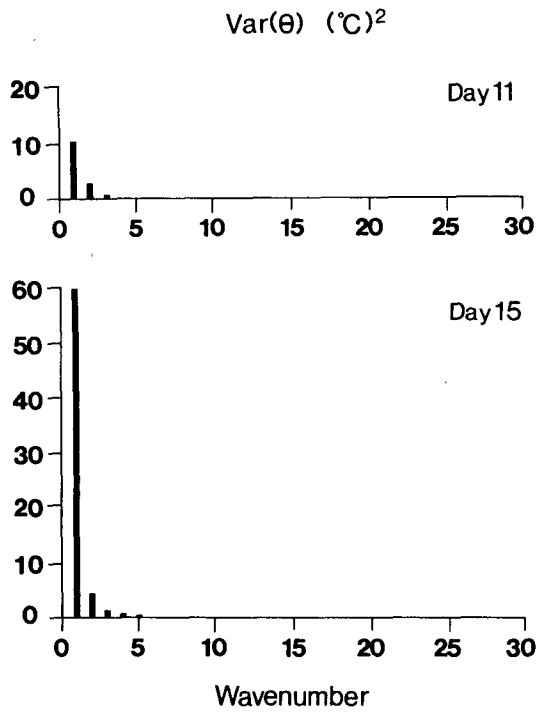

FIG. 20. As in Fig. 19 except for the case of Fig. 18.

solid line in Fig. 17a continues to grow linearly, but with a lower rate, until day 11 or so.

The drastic impact of the adjustment terms can be seen in Fig. 18. The initial linear growth of short waves is now completely eliminated, while they grow during the second half of the period presumably due to wave-wave interactions. On the other hand, the longest wave linearly grows until day 10 or so and again toward the end of the period.

Figure 19 shows the spectrum distribution of the potential temperature variance for day 11 and 15 obtained without the adjustment terms. The abscissa is the two-dimensional wavenumber given by $(m^2 + n^2Y^2/X^2)^{1/2}$, where X and Y are the domain size in the zonal and meridional directions, respectively. In this figure we have combined contributions from all waves whose two-dimensional wavenumbers belong to a unit interval centered at each integer value.

Drastic impact of the adjustment terms can again be seen in Fig. 20. Values associated with high wavenumbers (≥ 4 for day 11 and ≥ 6 for day 15) are now too small to be shown in the figure, which uses a linear scale for the variance. On the other hand, the variance associated with wavenumber 1 is much larger in Fig. 20 than in Fig. 19 on day 15. This is probably because more zonal available potential energy remains when the adjustment terms are included through suppressing the spurious conversion to short waves.

Up to this point, the results of the integrations are more or less what we can anticipate from the analysis of the linearized quasi-geostrophic model. The results shown in Figs. 21 and 22, however, reveal an additional effect of the spurious amplification of short waves. These figures show the distributions of potential temperature at selected levels of the model for day 11. Figure 21 shows that short waves are more dominant at

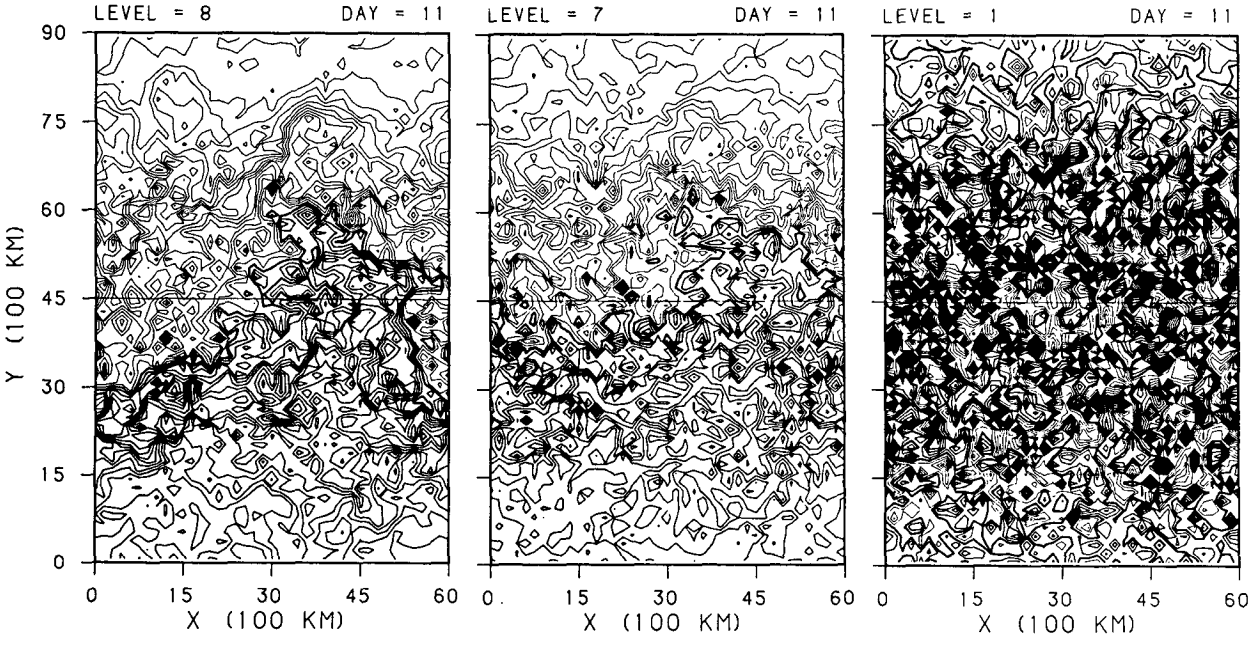

FIG. 21. The deviation of potential temperature from its area mean at level 8 (bottom layer), level 7 (layer immediately above bottom layer) and level 1 (top layer) for the case of Fig. 17. Contour interval is 3K. Heavy lines are for zero, medium lines for positive values, and thin lines for negative values.

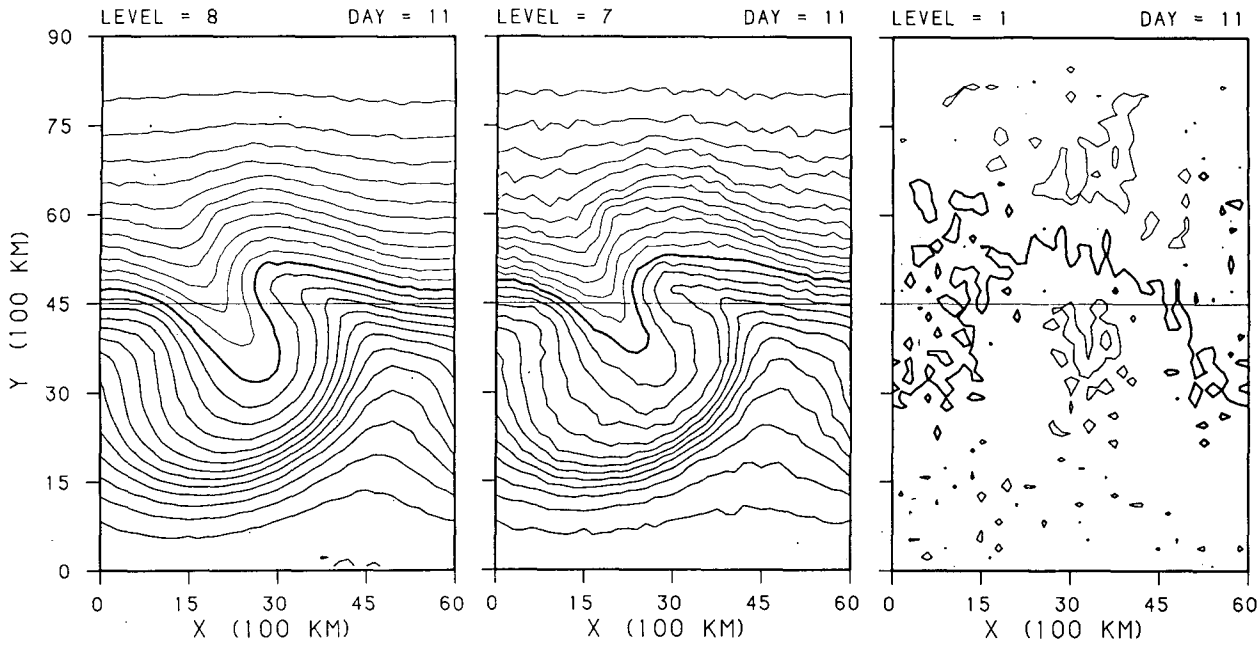

FIG. 22. As in Fig. 21 except for the case of Fig. 18.

the top level (level 1) than at lower levels (levels 8 and 7). This is opposite to what we expect from the analysis of the quasi-geostrophic system when the static stability parameter increases with height. Even for the primitive equation model, it is difficult to see why the growth rates due to in situ baroclinic instability are larger near the upper boundary than near the lower boundary. Therefore, we interpret the dominant short waves near the upper boundary as a consequence of the vertical propagation of gravity waves generated near the lower boundary as short waves amplify there.

9. Summary and discussion

With the Charney–Phillips vertical grid, one can easily maintain important dynamical constraints on quasi-geostrophic flow, such as the conservation of quasi-geostrophic potential vorticity through horizontal advection and resulting integral constraints. With the Lorenz vertical grid, however, it is not straightforward even to define quasi-geostrophic potential vorticity.

Using loosely defined quasi-geostrophic potential vorticity, we have pointed out that the Lorenz grid can falsely satisfy the necessary condition for baroclinic instability. In fact, growth-rate calculations show the existence of spuriously amplifying modes with short wavelength, one trapped near the lower boundary and the other near the upper boundary. The former grows more rapidly than the latter when the static stability parameter increases with height. The existence of the spurious amplification of short waves in a nonlinear primitive equation model has also been confirmed. Here the amplification also influences longer waves through nonlinearity and upper levels presumably through vertical propagation of gravity waves.

The system we have considered here is a physically unstable system, and it should be emphasized that the spurious amplification is not through computational instability in the ordinary sense. The amplification should be interpreted as a false realization of physical instability due to computational energy conversion, rather than a consequence of computational energy generation. The existence of lower (and upper) boundaries is crucial for the amplification, but the same is true for physical instability as well. Also, the amplifying mode should not be considered as a vertical computational mode. In the Lorenz grid, there is an extra degree of freedom in the vertical structure of potential temperature. Consequently, a model based on the Lorenz grid has a vertical computational mode in potential temperature, which is characterized by a quasi-stationary oscillation from level to level. At least in linearized cases, this computational mode is decoupled from all internal modes and, therefore, not subject to any kind of baroclinic instability. The extra degree of freedom in potential temperature, however, is indirectly responsible for the spurious amplification by producing an extra degree of freedom in potential vorticity.

The Lorenz grid is being widely used in existing primitive equation models. With this grid one can easily construct vertical difference schemes that conserve total energy, total enthalpy, and total entropy or total variance of enthalpy under adiabatic processes, as Lorenz did for the balanced model and as Arakawa (1972), and Arakawa and Lamb (1977) for the primitive equation model. While maintaining conservation of these quantities is desirable, it alone does not necessarily guarantee that dynamical processes responsible for energy conversions can be correctly simulated. The results

presented in this paper show that from the point of view of baroclinic instability, there are problems for short waves when the Lorenz grid is used. These problems appear in a model with *high* horizontal resolution unless vertical resolution is very high.

The spurious amplification of short waves should be more serious in a moist model, in which condensation resulting from low-level moisture convergence can give additional energy source. Moreover, owing to inherent nonlinearity, condensation processes associated with short waves can have significant impact on simulating large-scale fields. This impact can occur basically in two ways: through an increase in the overall amount of condensation when the moisture supply is unlimited; and through a decrease in the amount of moisture available for larger-scale condensation when the moisture supply is limited.

In spite of the problem pointed out in this paper, we are not suggesting that the Lorenz grid should be abandoned. The purpose of this paper is to advise that care must be taken in constructing high horizontal-resolution models with the Lorenz grid and in interpreting the results of such models. The same care must be taken in theoretical studies on subsynoptic-scale baroclinic instability, such as those on the effects of vertical and/or horizontal curvature of the basic wind profile and the effects of nongeostrophy and diabatic heating, whenever the Lorenz grid is used.

In a paper on baroclinic instability with cumulus heating, Moorthi and Arakawa (1985) showed the existence of a growing mode with short wavelengths, which they termed "*S*-mode." This mode, which was originally found by Shukla (1976, 1978) with a 3-level model, is different from the spuriously amplifying modes discussed in this paper. The *S*-mode can grow only with strong cumulus heating and can exist even in a model with low vertical resolution, such as that used by Shukla. Moorthi and Arakawa examined their 7-level model without cumulus heating and found that the model is almost free from the spurious amplification. This is because the model has a smaller value of f_0 and relatively low vertical resolution in the lower part of the model except for the bottom layer.

We have pointed out that the spurious amplification can be eliminated at its origin by including the terms (7.1) and (7.2) in the perturbation thermodynamic equations for the bottom and top layers. Inclusion of similar terms given by (8.1) and (8.2) in a nonlinear primitive equation model was also found to be effective. Since the spurious amplification of short waves is due to *baroclinic instability of computational kind* (BICK), these terms may be called "BICK-proof" terms. The formulation of BICK-proof terms presented here may not be the best, especially when the model includes boundary layer processes. We feel that in such models BICK-proof terms should be applied to a layer immediately above the boundary layer. In any case, the results presented in this paper are at least encouraging for continued use of the Lorenz grid.

Acknowledgments. We wish to thank Dr. Norman A. Phillips for his useful comments and an anonymous reviewer for the extensive and thorough review of this paper. We also thank Ms. Julia Lueken, Mrs. Clara Wong, and Ms. Mary Grace Bigornia for typing the manuscript and Ms. Mimi Archie for drawing the figures. This material is based on work supported jointly by NSF and NOAA under Grant ATM-8515013 and by NASA under Grant NAG 5-789.

REFERENCES

Arakawa, A., 1966: Computational design for long term numerical integration of the equations of fluid motion: Two-dimensional incompressible flow. Part I. *J. Comput. Phys.*, **1**, 119–143.

——, 1972: Design of the UCLA general circulation model. Numerical Simulation of Weather and Climate, Tech. Rep. No. 7, Dept. of Meteorology, University of California, 116 pp.

——, 1984: Vertical differencing of filtered models. *Numerical methods for weather prediction.* Vol. 1, *Seminar 1983, European Centre for Medium Range Weather Forecasting,* 183–206.

——, 1988: Finite-difference methods in climate modeling. *Physically Based Modeling and Simulation of Climate and Climate Change, Vol. I,* M. Schlesinger, Ed., D. Reidel, 79–168.

——, and V. R. Lamb, 1977: Computational design of the basic dynamical processes of the UCLA general circulation model. *Methods in Computational Physics,* Academic Press, 173–265.

——, and ——, 1981: A potential enstrophy and energy conserving scheme for the shallow water equations. *Mon. Wea. Rev.*, **109**, 18–36.

——, and M. J. Suarez, 1983: Vertical differencing of the primitive equations in sigma coordinates. *Mon. Wea. Rev.*, **111**, 34–45.

Bretherton, F. P., 1966: Critical layer instability in baroclinic flows. *Quart. J. Roy. Meteor. Soc.*, **92**, 325–334.

Charney, J. G., 1955: The use of primitive equations of motion in numerical prediction. *Tellus,* **7**, 22–26.

——, 1971: Geostrophic turbulence. *J. Atmos. Sci.*, **28**, 1087–1095.

——, and N. A. Phillips, 1953: Numerical integration of the quasi-geostrophic equations for barotropic and simple baroclinic flows. *J. Meteor.*, **10**, 71–99.

——, and M. Stern, 1962: On the stability of internal baroclinic jets in a rotating atmosphere. *J. Atmos. Sci.*, **19**, 159–172.

Eady, E. T., 1949: Long waves and cyclone waves. *Tellus,* **1**, 33–52.

Green, J. S. A., 1960: A problem in baroclinic stability. *Quart. J. Roy. Meteor. Soc.*, **86**, 237–251.

Hollingsworth, A., 1975: Baroclinic instability of a simple flow on the sphere. *Quart. J. Roy. Meteor. Soc.*, **101**, 495–528.

James, I. N., and B. J. Hoskins, 1985: Some comparisons of atmospheric internal and boundary baroclinic instability. *J. Atmos. Sci.*, **42**, 2142–2155.

Lorenz, E. N., 1955: Available potential energy and the maintenance of the general circulation. *Tellus,* **7**, 157–167.

——, 1960: Energy and numerical weather prediction. *Tellus,* **12**, 364–373.

Moorthi, S., and A. Arakawa, 1985: Baroclinic instability with cumulus heating. *J. Atmos. Sci.*, **42**, 2007–2031.

Pedlosky, J., 1964: An initial value problem in the theory of baroclinic instability. *Tellus,* **16**, 12–17.

Phillips, N. A., 1957: A coordinate system having some special advantages for numerical forecasting. *J. Meteor.*, **14**, 184–185.

Shukla, J., 1976: On the dynamics of monsoon depressions. Sc.D. thesis, Dept. of Meteorology, MIT, 178 pp.

——, 1978: CISK-barotropic-baroclinic instability and the growth of monsoon depressions. *J. Atmos. Sci.*, **35**, 495–508.

Suarez, M. J., A. Arakawa and D. A. Randall, 1983: The parameterization of the planetary boundary layer in the UCLA general circulation model: Formulation and results. *Mon. Wea. Rev.*, **111**, 2224–2243.

Tokioka, T., 1978: Some consideration on vertical differencing. *J. Meteor. Soc. Japan,* **56**, 89–111.